The high energy X-ray probe (HEX-P): probing the physics of the X-ray corona in active galactic nuclei

Elias Kammoun[1,2,3]*, Anne M. Lohfink[4], Megan Masterson[5], Dan R. Wilkins[6], Xiurui Zhao[7], Mislav Balokovic[8,9], Peter G. Boorman[10], Riley Connors[11], Paolo Coppi[12], Andrew Fabian[13], Javier A. García[10,14], Kristin K. Madsen[14], Nicole Rodriguez Cavero[15], Navin Sridhar[10,16], Daniel Stern[17], John Tomsick[18], Thomas Wevers[1,9], Dominic J. Walton[20], Stefano Bianchi[1], Johannes Buchner[21], Francesca M. Civano[14], Giorgio Lanzuisi[22], Labani Mallick[10,23,24], Giorgio Matt[1], Andrea Merloni[21], Emanuele Nardini[3], Joanna M. Piotrowska[10], Claudio Ricci[25,26], Ka-Wah Wong[27] and Abderahmen Zoghbi[28,29,30]

[1]Roma Tre University, Rome, Italy, [2]UMR5277 Institut de Recherche en Astrophysique et Planétologie (IRAP), Toulouse, France, [3]Osservatorio Astrofisico di Arcetri (INAF), Florence, Tuscany, Italy, [4]Department of Physics, College of Letters and Science, Montana State University, Bozeman, MT, United States, [5]MIT Kavli Institute for Astrophysics and Space Research, School of Science, Massachusetts Institute of Technology, Cambridge, MA, United States, [6]Kavli Institute for Particle Astrophysics and Cosmology, Stanford University, Stanford, CA, United States, [7]Center for Astrophysics, Harvard University, Cambridge, MA, United States, [8]Center for Astronomy and Astrophysics, Yale University, New Haven, CT, United States, [9]Department of Physics, Faculty of Arts and Sciences, Yale University, New Haven, CT, United States, [10]California Institute of Technology, Pasadena, CA, United States, [11]Department of Astrophysics and Planetary Science, Villanova University, Villanova, PA, United States, [12]Department of Astronomy, Faculty of Arts and Sciences, Yale University, New Haven, CT, United States, [13]Institute of Astronomy, Faculty of Physics and Chemistry, School of Physical Sciences, University of Cambridge, Cambridge, England, United Kingdom, [14]X-ray Astrophysics Laboratory, Goddard Space Flight Center, National Aeronautics and Space Administration, Greenbelt, MD, United States, [15]Department of Physics, Faculty of Arts and Sciences, Washington University in St. Louis, St. Louis, MO, United States, [16]Department of Astronomy, Columbia University, New York, NY, United States, [17]NASA Jet Propulsion Laboratory (JPL), La Cañada Flintridge, CA, United States, [18]Space Sciences Laboratory, University of California, Berkeley, Berkeley, CA, United States, [19]Space Telescope Science Institute (NASA), Baltimore, MD, United States, [20]Centre for Astrophysics Research, School of Physics Astronomy and Mathematics, University of Hertfordshire, Hatfield, United Kingdom, [21]Max Planck Institute for Extraterrestrial Physics, Garching, Germany, [22]Osservatorio di Astrofisica e Scienza dello Spazio di Bologna (INAF), Bologna, Emilia-Romagna, Italy, [23]University of Manitoba, Winnipeg, MB, Canada, [24]Department of Physics, Faculty of Arts and Science, Canadian Institute for Theoretical Astrophysics, University of Toronto, Toronto, ON, Canada, [25]Diego Portales University, Santiago, Chile, [26]The Kavli Institute for Astronomy and Astrophysics, School of Physics, Faculty of Science, Peking University, Beijing, China, [27]SUNY Brockport, Brockport, NY, United States, [28]Department of Astronomy, College of Computer, Mathematical and Natural Sciences, University of Maryland, College Park, College Park, MD, United States, [29]Goddard Space Flight Center, National Aeronautics and Space Administration, Greenbelt, MD, United States, [30]Center for Research and Exploration in Space Science and Technology, University of Maryland, College Park, Greenbelt, MD, United States

The hard X-ray emission in active galactic nuclei (AGN) and black hole X-ray binaries is thought to be produced by a hot cloud of electrons referred to as the corona. This emission, commonly described by a power law with a high-energy cutoff, is suggestive of Comptonization by thermal electrons. While several hypotheses have been proposed to explain the origin, geometry,

and composition of the corona, we still lack a clear understanding of this fundamental component. *NuSTAR* has been playing a key role improving our knowledge of X-ray coronæ thanks to its unprecedented sensitivity above 10 keV. However, these constraints are limited to bright, nearby sources. The *High Energy X-ray Probe* (*HEX-P*) is a probe-class mission concept combining high spatial resolution X-ray imaging and broad spectral coverage (0.2–80 keV) with a sensitivity superior to current facilities. In this paper, we highlight the major role that *HEX-P* will play in further advancing our insights of X-ray coronæ notably in AGN. We demonstrate how *HEX-P* will measure key properties and track the temporal evolution of coronæ in unobscured AGN. This will allow us to determine their electron distribution and test the dominant emission mechanisms. Furthermore, we show how *HEX-P* will accurately estimate the coronal properties of obscured AGN in the local Universe, helping address fundamental questions about AGN unification. In addition, *HEX-P* will characterize coronæ in a large sample of luminous quasars at cosmological redshifts for the first time and track the evolution of coronæ in transient systems in real time. We also demonstrate how *HEX-P* will enable estimating the coronal geometry using spectral-timing techniques. *HEX-P* will thus be essential to understand the evolution and growth of black holes over a broad range of mass, distance, and luminosity, and will help uncover the black holes' role in shaping the Universe.

1 Introduction

Active galactic nuclei (AGN) are known to be prolific X-ray emitters. The hard X-rays from AGN are thought to be generated through Compton scattering of thermal UV-soft X-ray seed photons from the accretion disk by a hot electron plasma located in the vicinity of the black hole, known as the corona (e.g., Vaiana and Rosner, 1978; Rybicki and Lightman, 1979; Haardt and Maraschi, 1991; 1993). The resulting X-ray continuum spectrum is usually approximated by a power law of photon index Γ, with a high-energy cutoff (E_{cut}) at tens to hundreds of keV (e.g., Fabian et al., 2017; Tortosa et al., 2018; 2023). Within the Comptonization framework, Γ and E_{cut} can be mapped into the electron temperature[1] (kT_e) and the coronal optical depth (τ) plane (see, e.g., Titarchuk and Lyubarskij, 1995; Zdziarski et al., 1996; Beloborodov, 1999; Petrucci et al., 2001a; b; Middei et al., 2019). The X-ray corona thus holds key information about the physical processes occurring near the supermassive black hole (SMBH), offering insights into the energetic phenomena associated with AGN. Understanding the physics of the X-ray corona in AGN is crucial for unraveling the accretion process, comprehending the origin of the emission from AGN, studying black hole feedback and its impact on galaxy evolution, probing strong gravity regimes, and investigating magnetic fields and particle acceleration.

1.1 The geometry of the X-ray corona

Constraining the geometry (e.g., size and location) of the X-ray corona offers an opportunity to test models for the formation of the corona as each mechanism predicts a distinct geometry. For example, the "two-phase" corona model proposed by Haardt and Maraschi (1991) predicts an extended corona. In contrast, within the framework of the failed jet model proposed by Ghisellini et al. (2004), the corona is expected to be compact. To date, the most promising constraints come from microlensing variability. The microlensing of quasars by stellar components in the lensing galaxy results in a complex magnification pattern (e.g., Wambsganss, 2006). The relative motion of the lensed quasar, the galaxy and its stellar components, and the observer leads to uncorrelated variability. The variability amplitude depends significantly on the size of the emitting region, with a larger amplitude from a smaller emitting region. Thus, the size of the source region can be estimated by modelling the light curve of a lensed quasar (e.g., Chartas et al., 2002; Kochanek et al., 2007; Chartas et al., 2009; Mosquera et al., 2013; Chartas et al., 2016). Reis and Miller (2013) compiled measurements of the X-ray-emitting region in lensed quasars and found the sizes range from ~ one to tens of gravitational radii ($r_g = GM_{BH}/c^2$, where G is the gravitational constant, M_{BH} is the mass of the black hole, and c the speed of light). We highlight that current results are based on only a few strongly lensed quasars.

X-ray spectral and spectral-timing properties of nearby bright Seyfert galaxies, notably the detection of X-ray reverberation lags, led to the similar conclusion that the X-ray source is compact and lies within a few gravitational radii of the black hole (Fabian et al., 2009;

---

[1] The cutoff energy is commonly estimated to be ~2 – 3 times the electron temperature (Petrucci et al., 2001a).

De Marco et al., 2013; Cackett et al., 2014; Emmanoulopoulos et al., 2014; Uttley et al., 2014; Kara et al., 2016). Modelling the continuum optical-to-X-ray spectral energy distribution (SED) of a few bright Seyfert galaxies also yields similar estimates of the corona size (e.g., Done et al., 2013; Petrucci et al., 2013; Porquet et al., 2019). This has been recently applied also to a bright quasar at intermediate redshift (Kammoun et al., 2023). Further evidence of a small physical size of the corona emerges from varying obscuration of the corona by clouds in the broad line region (e.g., Risaliti et al., 2011; Sanfrutos et al., 2013; Gallo et al., 2021). These results motivated the adoption of the lamp-post geometry to describe the disk–corona system, where the X-ray corona is assumed to be a point-like source located on the symmetry axis of the disk (e.g., Matt et al., 1991; Martocchia and Matt, 1996; Miniutti and Fabian, 2004). Such a geometry could be physically realized by collisions and shocks within an ejection flow or a failed jet (e.g., Henri and Pelletier, 1991; Henri and Petrucci, 1997; Ghisellini et al., 2004), and has been assumed in detailed models for the calculation of reflection spectra (e.g., Dauser et al., 2013; García et al., 2014; Niedźwiecki et al., 2016; Ingram et al., 2019; Mastroserio et al., 2021; Dovčiak et al., 2022). We note that recently several works are considering a variety of more realistic 3D coronal geometries (e.g., Wilkins et al., 2016; Gonzalez et al., 2017; Zhang W. et al., 2019).

Several works have adopted an approach similar to the one of Soltan (1982) to constrain the radiative efficiency (η) of accreting SMBHs (e.g., Fabian and Iwasawa, 1999; Yu and Tremaine, 2002; Marconi et al., 2004; Shankar et al., 2004; 2009; 2020; Raimundo and Fabian, 2009; Raimundo et al., 2012; Aversa et al., 2015; Zhang and Lu, 2017). This cosmology-independent approach enables constraining the radiative efficiency by comparing the energy density of quasar/AGN radiation with the local mean SMBH mass density. All these works resulted in constraining η to be larger than 0.1. More recently, Shankar et al. (2020) favor $\eta \sim 0.12$–0.2 which is in line with spinning SMBH, suggesting an average spin value larger than ~0.5. For these spin values half of the accretion disk emission is produced within the inner $20r_g$ (see, e.g., Agol and Krolik, 2000; Dovčiak et al., 2022). The inner edge of the accretion disk is thus required to extend close to the black hole. Consequently, the bulk of the emission should be emitted from a compact region, which is in agreement with the results obtained from X-ray observations.

1.2 The heating and cooling mechanisms of the X-ray corona

While the heating mechanism of the corona is still uncertain, magnetic reconnection has been suggested to play an important role (e.g., Galeev et al., 1979; Di Matteo et al., 1997; Merloni and Fabian, 2001a; b; Sironi and Beloborodov, 2020; Sridhar et al., 2021; 2023; Gupta et al., 2023). Within this scenario, the magnetized coronæ could generate cyclo/synchrotron radiation that can be observed in the radio/mm band (e.g., Laor and Behar, 2008; Inoue and Doi, 2014; Panessa et al., 2019). In fact, low levels of radio emission has been almost ubiquitously detected in radio-quiet AGN. In many cases, the emitting region is unresolved and associated with a compact, sub-kpc nuclear region (see, e.g., Smith et al., 2016; Panessa et al., 2019,

and references therein). Given the expected physical size of the X-ray emitting region, the coronal mm-wave synchrotron emission is expected to be self-absorbed, and it would therefore be more easily detectable in the mm than in the radio. The size (R) of the self-absorbed synchrotron source decreases with frequency following $R \propto \nu^{-7/4}$. Thus, the synchrotron emission from an X-ray corona sized source would peak at ~100 GHz (e.g., Raginski and Laor, 2016; Inoue and Doi, 2018). Several observational studies hint towards a coronal origin of the mm-wave nuclear emission in non-jetted AGN (e.g., Behar et al., 2015; 2018; Doi and Inoue, 2016; Inoue and Doi, 2018; Kawamuro et al., 2022; 2023; Petrucci et al., 2023). In particular, correlations between mm continuum emission and X-ray emission have been found in various samples of AGN, with an average ratio between the ~100 – 200 GHz and X-ray continuum of ~10^{-5} – 10^{-4} (Behar et al., 2015; 2018; Kawamuro et al., 2022; Ricci et al., 2023). Interestingly, this relation is consistent with what has been observed in coronally active stars (Guedel and Benz, 1993), which are magnetically heated, similar to what is expected for AGN coronæ, further supporting the proposed coronal origin for the 100–200 GHz continuum emission, and in turn the idea that the corona is magnetically heated.

A physically compact X-ray corona is expected to be radiatively compact, meaning that the luminosity to radius ratio (L/R_c) is large. The compactness is usually described by the dimensionless parameter $\ell = \frac{L}{R_c} \frac{\sigma_T}{m_e c^3}$, where σ_T is the Thompson scattering cross section and m_e is the electron mass (Guilbert et al., 1983). For large values of ℓ, the number density of the high-energy photons can lead to electron-positron pair production due to photon-photon collisions. In this case, feeding the corona with more energy will lead to the production of more particles to share the energy, which will limit the increase of the temperature of the corona and prevent pair production from becoming a runaway process and exceed annihilation. This can be assimilated to an ℓ-dependent thermostat (Svensson, 1984; Zdziarski and Lightman, 1985; Stern et al., 1995). Observational constraints on the coronal parameters so far obtained are in agreement with the hypothesis that pair production and annihilation may act as an effective thermostat controlling the coronal temperature (Fabian et al., 2015; 2017). It is common to assume that the coronal plasma is thermal. However, several AGN show electron temperatures that are much lower than expected for a purely thermal pair plasma (see, e.g., Baloković et al., 2015; Ursini et al., 2016; Kara et al., 2017; Tortosa et al., 2018; Reeves et al., 2021; Bertola et al., 2022). These low temperatures could be indicative of a hybrid plasma composed of a mixture of thermal and non-thermal particles (Ghisellini et al., 1993; Zdziarski et al., 1993; Fabian et al., 2017). Only a small fraction of non-thermal electrons with energy above 1 MeV would be needed to result in runaway pair production. In this case, the cooled pairs share the energy which reduces the temperature of the corona.

It is common to model the Comptonization spectrum using a phenomenological power law with a high energy cutoff. Various physical models are also used and all of them describe the current data equally well. These models differ in their assumptions for the spectrum of the seed photons and the geometry of the Comptonizing region. Various analytic Comptonization models such as CompTT (Titarchuk, 1994) and CompPS (Poutanen and Svensson, 1996) are used, allowing different simple geometries. Recently, more physically

self-consistent calculations such as EQPAIR (Coppi, 1999), BELM (Belmont et al., 2008), MoCa (Tamborra et al., 2018), and MONK (Zhang W. et al., 2019) include a variety of geometries, hybrid coronæ, and polarization.

1.3 Observational constraints

The unprecedented sensitivity of *NuSTAR* (Harrison et al., 2013) above 10 keV has been instrumental to study the hard X-ray spectra of AGN. *NuSTAR* enabled high-energy cut-off measurements from single epoch observations for a relatively large sample of local (Ballantyne et al., 2014; Matt et al., 2014; Baloković et al., 2015; 2020; Ricci et al., 2017; Tortosa et al., 2018; Akylas and Georgantopoulos, 2021; Kamraj et al., 2022; Tortosa et al., 2023) and intermediate-redshift AGN for the first time (see, e.g., Kammoun et al., 2017; 2023; Lanzuisi et al., 2019; Bertola et al., 2022; Marinucci et al., 2022b, and references therein). It should be mentioned that previous studies (with *BeppoSAX, RXTE, INTEGRAL*, etc.) allowed these measurements for a much smaller sample of the brightest nearby AGN (e.g., Nicastro et al., 2000; Petrucci et al., 2004; Malizia et al., 2014; Lubiński et al., 2016). *NuSTAR* observations allowed us not only to constrain the coronal temperature by accurately measuring values of $E_{\rm cut}$, but also to probe its variability (e.g., Ballantyne et al., 2014; Zoghbi et al., 2017) the origin of which remains unclear.

The *Swift*/BAT AGN sample comprises all AGN detected by the all-sky 14–195 keV BAT survey (Baumgartner et al., 2013; Oh et al., 2018). Ricci et al. (2017) have estimated a median high-energy cutoff of local unobscured AGN (i.e., $\log\left(N_{\rm H}/{\rm cm}^{-2}\right) <$ 22) of $E_{\rm cut} = 210 \pm 36$ keV. Ricci et al. (2018) subsequently found evidence for an inverse correlation between $E_{\rm cut}$ and Eddington ratio ($\lambda_{\rm Edd}$) where the median $E_{\rm cut}$ increases from $E_{\rm cut} = 160 \pm 41$ keV to $E_{\rm cut} = 370 \pm 51$ keV considering AGN with $\lambda_{\rm Edd}$ larger and smaller than 0.1, respectively. This could be suggestive that the properties of the X-ray corona evolve with the accretion rate. More recently, Kamraj et al. (2022) included *NuSTAR* observations of this sample and estimated the mean electron temperature to be $kT_{\rm e} = 84 \pm 9$ keV, which is consistent with the values reported previously in the literature. However, the authors were not able to recover the correlation between the electron temperature and any of the accretion parameters. It is worth mentioning that differences in coronal spectra may be expected between obscured and unobscured AGN, within the framework of the orientation-based unified model of AGN (Antonucci, 1993; Urry and Padovani, 1995), especially if the corona has a net velocity perpendicular to the accretion disk (most likely related to jet formation; see, e.g., Malzac et al., 2001; Markoff et al., 2005). However, Baloković et al. (2020) estimated a median $E_{\rm cut} = 290 \pm 20$ keV for a sample of 130 local obscured AGN, consistent within the current large uncertainties with the values found by Ricci et al. (2017) for unobscured AGN.

More recently, the launch of the *Imaging X-ray Polarimetry Explorer* (*IXPE*; Weisskopf et al., 2022) has enabled studies of X-ray polarization in AGN for the first time (in the 2–8 keV range). X-ray polarization is a powerful technique to explore the geometry of the X-ray emitting region (see, e.g., Schnittman and Krolik, 2010; Beheshtipour et al., 2017; Tamborra et al., 2018;

Zhang W. et al., 2019). So far, a total of four non-blazar AGN have been observed (NGC 4151, MCG–05-23-16, the Circinus galaxy, and IC 4329A). Only upper limits could be determined for MCG–05-23-16 (Marinucci et al., 2022b; Tagliacozzo et al., 2023) and IC 4329A (Ingram et al., 2023), which are not conclusive on the geometry of the X-ray source. The Circinus galaxy shows a polarization of 28 ± 7 per cent (at 68 per cent confidence level), with a polarization angle of $18° \pm 5°$, roughly perpendicular to the radio jet (Ursini et al., 2023). Given the large obscuration in this source, this polarization is most likely due to reflection off cold material in the torus (e.g., Ghisellini et al., 1994; Goosmann and Matt, 2011; Marin et al., 2018; Ratheesh et al., 2021) and cannot be interpreted as the intrinsic polarization of the X-ray source. As for NGC 4151, a polarization of 4.9 ± 1.1 per cent with a polarization angle of $86° \pm 7°$ (at the 68 per cent confidence level) are reported by Gianolli et al. (2023). This is consistent with a radially extended source of polarization that is perpendicular to the radio jet, i.e., parallel to the accretion disk. Similar results have also been observed in the black hole X-ray binary Cygnus X-1 (Krawczynski et al., 2022).

The *High-Energy X-ray Probe* (*HEX-P*; Madsen et al., 2023; in preparation) will address many of the open questions related to the physics of the X-ray corona in AGN. In this paper, we showcase how *HEX-P* will play a major role in advancing our understanding of the physics of the X-ray coronæ in AGN. In Section 2 we briefly present the properties of the mission. Characterisations of the X-ray coronæ in unobscured and obscured AGN with *HEX-P* are discussed in Section 3 and Section 4, respectively. Section 5 shows how studying the X-ray coronæ in high-redshift quasars will be possible with *HEX-P*. Section 6 addresses the capabilities of *HEX-P* in studying the X-ray coronæ of transient sources. Section 7 demonstrates how *HEX-P* will allow us to better constrain the coronal geometry. Finally, we present a summary and a brief discussion in Section 9.

2 Mission design

HEX-P is a probe-class mission concept that offers sensitive broad-band coverage (0.2–80 keV) of the X-ray spectrum with exceptional spectral, timing, and angular capabilities. It features two high-energy telescopes (HETs) that focus hard X-rays, and one low-energy telescope (LET) that focuses lower energy X-rays.

The LET consists of a segmented mirror assembly coated with Ir on monocrystalline silicon that achieves a half power diameter of $3.5''$, and a low-energy DEPFET detector, of the same type as the Wide Field Imager (WFI; Meidinger et al., 2020) onboard *Athena* (Nandra et al., 2013). It has 512×512 pixels that cover a field of view of $11.3' \times 11.3'$. It has an effective passband of 0.2–20 keV, and a full frame readout time of 2 ms, which can be operated in a 128 and 64 channel window mode for higher count-rates to mitigate pile-up and faster readout. Pile-up effects remain below an acceptable limit of ~1% for fluxes up to ~100 mCrab in the smallest window configuration. Excising the core of the PSF, a common practice in X-ray astronomy, will allow for observations of brighter sources, with a typical loss of up to ~60% of the total photon counts.

The HET consists of two co-aligned telescopes and detector modules. The optics are made of Ni-electroformed full shell mirror

substrates, leveraging the heritage of *XMM-Newton* (Jansen et al., 2001), and coated with Pt/C and W/Si multilayers for an effective passband of 2–80 keV. The high-energy detectors are of the same type as flown on *NuSTAR* (Harrison et al., 2013), and they consist of 16 CZT sensors per focal plane, tiled 4×4, for a total of 128×128 pixels spanning a slightly larger field of view than the LET, $13.4' \times 13.4'$.

The broad X-ray band pass and superior sensitivity will provide a unique opportunity to study the X-ray corona physics across a wide range of energies, luminosity, and dynamical regimes.

2.1 Simulations

All the simulations presented here were produced with a set of response files that represent the observatory performance based on current best estimates (see Madsen et al., 2023; in preparation). The effective area is derived from a ray-trace of the mirror design including obscuration by all known structures. The detector responses are based on simulations performed by the respective hardware groups, with an optical blocking filter for the LET and a Be window and thermal insulation for the HET. The LET background was derived from a GEANT4 simulation (Eraerds et al., 2021) of the WFI instrument, and the HET background was derived from a GEANT4 simulation of the *NuSTAR* instrument; both simulations assume *HEX-P* is orbiting at the first Earth-Sun Lagrangian point (L1).

3 Physics of the corona in unobscured AGN

Unobscured AGN $(\log\left(N_{\mathrm{H}}/\mathrm{cm}^{-2}\right) < 22)$ with their clean view of the central engine have provided most of the knowledge we have today regarding AGN coronæ, as outlined in Section 1. The view of the whole Comptonization spectrum, and of the X-ray reflection arising from the interaction with the disk, is what makes X-ray observations of unobscured AGN so valuable. The constraints provided on these sources are key as we move towards refining our picture of AGN coronæ with *HEX-P*.

NuSTAR observations of unobscured AGN have provided many coronal temperature measurements, which are consistent with the runaway pair production scenario discussed above. Interestingly, in some AGN the coronal temperatures have been found to be much lower than what would be expected for pair-regulated thermal coronæ. One likely explanation for this is that the energy distribution of the electrons in the corona is not entirely thermal but has a non-thermal contribution. Such a hybrid corona would have a lower observed coronal temperature as the non-thermal high energy electrons create pairs even when the bulk of the electrons have lower temperatures.

The hybrid nature of the electron distribution can be detected directly from the X-ray spectrum. Comptonization from thermal electrons results in a power-law like X-ray continuum with a fairly abrupt cut-off at high energies. Consequently, an addition of non-thermal electrons, following a power-law like distribution beyond the thermal peak, leads to an increase in hard X-rays, as there are now electrons with even higher energies. This additional hard

X-ray emission beyond the thermal cut-off is usually referred to as a "hard tail".

Using these differences in the resulting Comptonization spectrum, i.e., the X-ray continuum, some evidence has been found in black hole X-ray binaries that the X-ray continuum is caused by hybrid Comptonization (e.g., Cadolle Bel et al., 2006; Cangemi et al., 2021; Zdziarski et al., 2021). The presence of hybrid Comptonization in AGN has been widely hypothesized but a direct detection of the hard tail itself is beyond the capabilities of current and proposed future instruments. *HEX-P*, however, will allow indirect confirmation of the presence of hybrid Comptonization in AGN and determine the strength of its contribution.

There are two primary methods to indirectly detect hybrid Comptonization: one relies on the reflection spectrum of the high energy continuum (García et al., 2015, see also Section 9), and the other tests temperature regulation by electron-positron pair production. The latter case can be made by studying the evolution of a source with unusually low coronal temperature over a period of time. If the source is variable, we can study the evolution of its compactness and coronal temperature with time. If the coronal temperature is set by pair production and the accretion geometry remains unchanged[2] then as the source flux increases, the coronal temperature will decrease. If, on the other hand, the coronal temperature is not regulated by pairs then the temperature may not change or change in a different fashion. If we see the expected trend of lower coronal temperature with increased flux, and if the observed coronal temperatures are much lower than expected for thermal Comptonization, that would be strongly indicative of hybrid Comptonization. The findings can then also be compared to theoretical predictions. In rare cases, this is already possible with today's instrumentation for some of the brightest X-ray binaries (see Buisson et al., 2019, for an example), but has remained out of reach for AGN. For the observations to yield meaningful constraints our measurements need to be more accurate at low fluxes than is possible with current instruments. However, *HEX-P* is able to obtain much tighter constraints on the coronal temperatures due to its low background at high energies (Figure 1, left), enabling a high-quality study of coronal temperature variations in AGN for the first time.

To demonstrate this, we explored the feasibility of a study with *HEX-P* that targets the evolution of the coronal temperature in the bright, local narrow-line Seyfert 1 galaxy Ark 564. Ark 564 is ideally suited for such a study as it exhibits a low measured coronal temperature (Kara et al., 2017; Lewin et al., 2022) as well as observed coronal temperature and flux variations (Barua et al., 2020). Our *HEX-P* simulations of Ark 564 are based on the absorbed 2–10 keV fluxes observed with *RXTE* over a 4-year period ranging from 1999 to 2003 and our simulations are further assuming a scenario where the coronal size remains unchanged with luminosity[3]. During this period the observed 2–10 keV flux varies between 1.0–5.0×10^{-11} *erg s*$^{-1}$ *cm*$^{-2}$ (Rivers et al., 2013). We simulate spectra at five evenly spaced levels within the observed flux range assuming a model that consists of a thermal

---

2   This can be assessed by studying the X-ray reflection spectrum.

3   Our final conclusions do not depend on this assumption, as the coronal size can also be estimated from the spectral modeling.
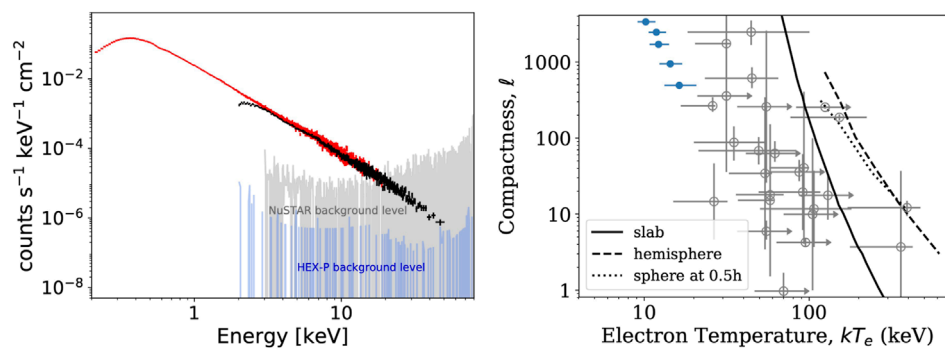
FIGURE 1
Left: Simulated LET (red) and HET (black) spectra of Ark 564, assuming Γ =2.48, kT_e = 13 keV and an exposure time of 90 ks. The figure also shows the background levels of *NuSTAR* (grey) and *HEX-P*-HET (blue): the background of *HEX-P* is significantly lower than that of *NuSTAR*. Right: Corona compactness as function of electron temperature. The blue circles correspond to simulated observations of Ark 564 with *HEX-P* at five different flux levels and five different coronal temperatures from 15 to 10 keV (see text). For clarity, uncertainities in the compactness of Ark 564 are not plotted. The grey empty circles represent typical estimates of kT_e from other AGN performed with *NuSTAR*.

Comptonization continuum and its associated reflection spectrum, both of which are treated with the relativistic reflection model `relxilllpcP` (Dauser et al., 2020). The second lowest flux level of 2.0×10^{-11} erg s^{-1} cm^{-2} corresponds very well to the 2018 joint *XMM-Newton + NuSTAR* observations of the source, which were studied in detail in Lewin et al. (2022). We therefore adopt the spectral parameters from their detailed modeling for this flux level (Table 3 in their paper), in particular they have determined that $\Gamma = 2.48$ and $kT_e = 14.7$ keV at this particular flux level. Then as we vary the flux level, we not only adjust the normalization of our spectral model but also evolve the photon index from 2.40 to 2.56 to mimic a softer-when-brighter effect and the coronal temperature from 15.1 to 10.0 keV to have the coronal evolve mildly with flux, the reflection parameters are kept unchanged. To determine how much exposure time was needed at each flux level, we simulated spectra with increasingly longer exposure times until we were able to recover the coronal temperature with an accuracy of ±2.5 keV or better at 90% confidence. From the simulations, we found that a study of Ark 564 with *HEX-P* with a total exposure time of 445 ks targeting the source at different flux levels will constrain the coronal temperature to ≤2.5 keV and could yield important data points in the compactness-temperature plane (blue points, Figure 1, right). At higher flux levels it is easy for us to exceed the accuracy requirement of 2.5 keV and the error bars are therefore smaller. We note here that accuracy of the coronal temperature constraint for a certain simulated exposure time is model-dependent, where more complex models lead to less accurate constraints.

To place the findings from the Ark 564 study into the context of the wider population of radio-quiet, unobscured AGN, ideally a few similar studies of other sources would also be conducted. Suitable study targets display large variability on timescales of weeks to months and possess a low coronal temperature, several of such sources have already been identified. Together, with the findings from one-time observation of unobscured AGN and high redshift targets, this will highlight whether Ark 564 is special in any way or whether its coronal variations can be considered representative for the population as a whole.

The much lower background of *HEX-P* at higher energies and the therefore much improved constraints on the spectral shape in this energy range with shorter exposure times will likely not only lead to a better understanding of hybrid Comptonization, but also to a more accurate spectral decomposition of unobscured AGN. This aspect is studied in more detail in Piotrowska et al. (2023).

4 Physics of the corona in obscured AGN

Within the framework of the orientation-based unified model for AGN (Antonucci, 1993), differences in coronal spectra between obscured $(\log(N_H/\text{cm}^{-2}) \geq 22)$ and unobscured AGN could be expected if the corona has significant velocity perpendicular to the accretion disk, possibly related to jet formation (Beloborodov, 1999; Markoff et al., 2005; Liu et al., 2014). Hard X-rays (≥15 keV) are essential to study the intrinsic properties of obscured AGN, as the obscuring material is optically thin to these photons. Constraints on coronæ in obscured AGN remain extremely scarce in the literature despite the prevalence of obscured AGN both in the local universe and, particularly, at high redshift (50%–75% of the population; Hickox and Alexander, 2018). A few constraints based on data from non-focusing hard X-ray instruments are available from, e.g., *BeppoSAX* (Dadina, 2007), *Suzaku* (Tazaki et al., 2011), *INTEGRAL* (de Rosa et al., 2012), *Swift*/BAT (Ricci et al., 2018), or a combination thereof (Molina et al., 2013). However, the cutoff of the power-law continuum at high energies, E_{cut}, has been well constrained using *NuSTAR* data for only about a dozen bright, obscured AGN (e.g., Baloković et al., 2015; Fabian et al., 2017; Buisson et al., 2018; Tortosa et al., 2018; Ursini et al., 2019), while larger samples representative of the obscured AGN population provide ensemble-level constraints mostly based on short *NuSTAR* observations with limited photon statistics (Baloković et al., 2020). In addition to E_{cut}, we note that constraining the photon index in obscured AGN is crucial to study the intrinsic AGN spectrum and understand the accretion process.

Thanks to its low background, and broad-band energy coverage, *HEX-P* will provide better constraints on the properties of the X-ray corona in obscured AGN. We performed simulations of various configurations of absorbed AGN to test the capabilities of *HEX-P* in constraining coronal parameters, assuming uniform exposure times of 100 ks (typical exposure for the planned *HEX-P* surveys; see Civano et al., 2023). We used the borus02 model (Baloković et al., 2018), which self-consistently computes the reprocessed emission from a sphere with conical cutouts at both poles, approximating a torus with variable covering factor. We considered a torus with a half-opening angle of 45° and an inclination of 60°. We also considered a photon index of the incident power law of $\Gamma = [1.6, 1.9, 2.2]$, and a high-energy cutoff

$E_{cut} = [50, 150, 300]$ keV. The incident luminosity was estimated to match the average values observed by Ricci et al. (2017) for $z = 0.02$ and $z = 0.5$, resulting in unabsorbed 2–10 keV luminosities in the range $10^{42.9-45.5}$ erg s^{-1}. We considered three values for the column densities $\log(N_H/cm^{-2}) = [22, 23, 24]$. For simplicity, we assume a homogeneous torus with the line-of-sight column density equal to the equatorial value. In addition, the soft X-ray spectrum in obscured AGN is typically characterized by the emission from photoionized gas in the narrow line region. For simplicity, we include a soft APEC component, which is commonly used in the literature to model this emission in absorbed AGN. For this component we assume a temperature of 0.9 keV and a normalization that is equal to 10% that of the power law, as
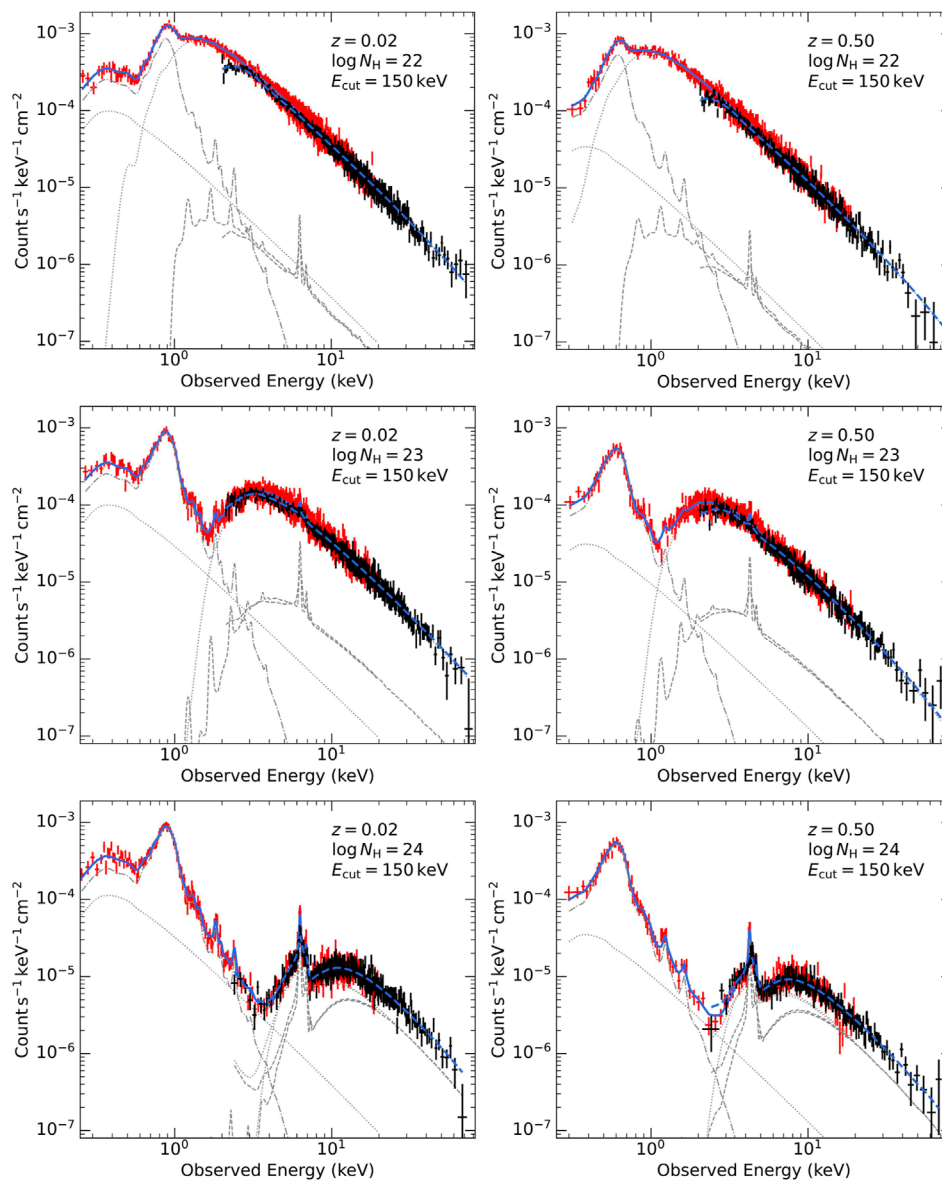
FIGURE 2
Simulated LET (red) and HET (black) spectra of an absorbed AGN at $z = 0.02$ (left) and $z = 0.5$ (right), assuming $\log(N_H/cm^{-2}) = 22, 23, 24$ (top to bottom), $\Gamma = 1.9$, $E_{cut} = 150$ keV, and an exposure time of 100 ks. The grey dotted lines represent the power law components, the grey dashed lines represent the neutral reflection component, and the grey dash-dotted lines represent the thermal component.

typically seen in local AGN (see, e.g., Kammoun et al., 2020). The total model results observed 2–10 keV fluxes in the range 2.5–8.5×10^{-12} erg s^{-1} cm^{-2} Figure 2 shows example *HEX-P* spectra for an intermediate configuration for all the simulated N_H values, assuming $\Gamma = 1.9$, and $E_{cut} = 150$ keV, for $z = 0.02$ and $z = 0.5$ (left and right panels, respectively). Figure 3 shows the E_{cut}-vs-Γ contours at the 3σ confidence level for all the configurations considered. *HEX-P* accurately measures the photon index over a broad range of parameters. The uncertainty on Γ is larger for higher column densities, since increasing amounts of absorption limits the access to the power law portion of the continuum to increasingly hard X-rays. This yields larger uncertainties on E_{cut} as well. The uncertainty on E_{cut} also increases with increasing E_{cut}; only lower limits could be estimated for $E_{cut} = 300$ keV. We note that the observed flux decreases by a factor of ~3 between $z = 0.02$ and $z = 0.5$, which lead to an increase in the uncertainty on the parameters higher redshift. For comparison with current facilities, we simulate a joint 30-ks *XMM-Newton* plus 100-ks *NuSTAR* (accounting for

both modules, FPMA and FPMB) observation, which are typical exposures with these facilities. For all cases, we adopt $z = 0.02$ as it results in tighter constraints than the $z = 0.5$ case. The $\Gamma - E_{cut}$ constraints are shown as black dotted contours in Figure 3, demonstrating the improvements enabled by *HEX-P*. We note that, for the flux levels of these sources and the exposure time, many of these sources will be easily detected in the *HEX-P* surveys (see Civano et al., 2023).

We would like to note that our `borus02` model is setup in coupled mode in which the line-of-sight and global column densities scale together. The reflection component will be higher at higher line-of-sight column densities, possibly contributing to the increased uncertainties in the higher N_H regime that we show in Figure 3. To definitively test this would require knowledge of the dependence between global column density and a wide range of different physical AGN parameters as well as a wide range of different model prescriptions for the obscurer, which is outside the scope of the current work. It is also worth mentioning that
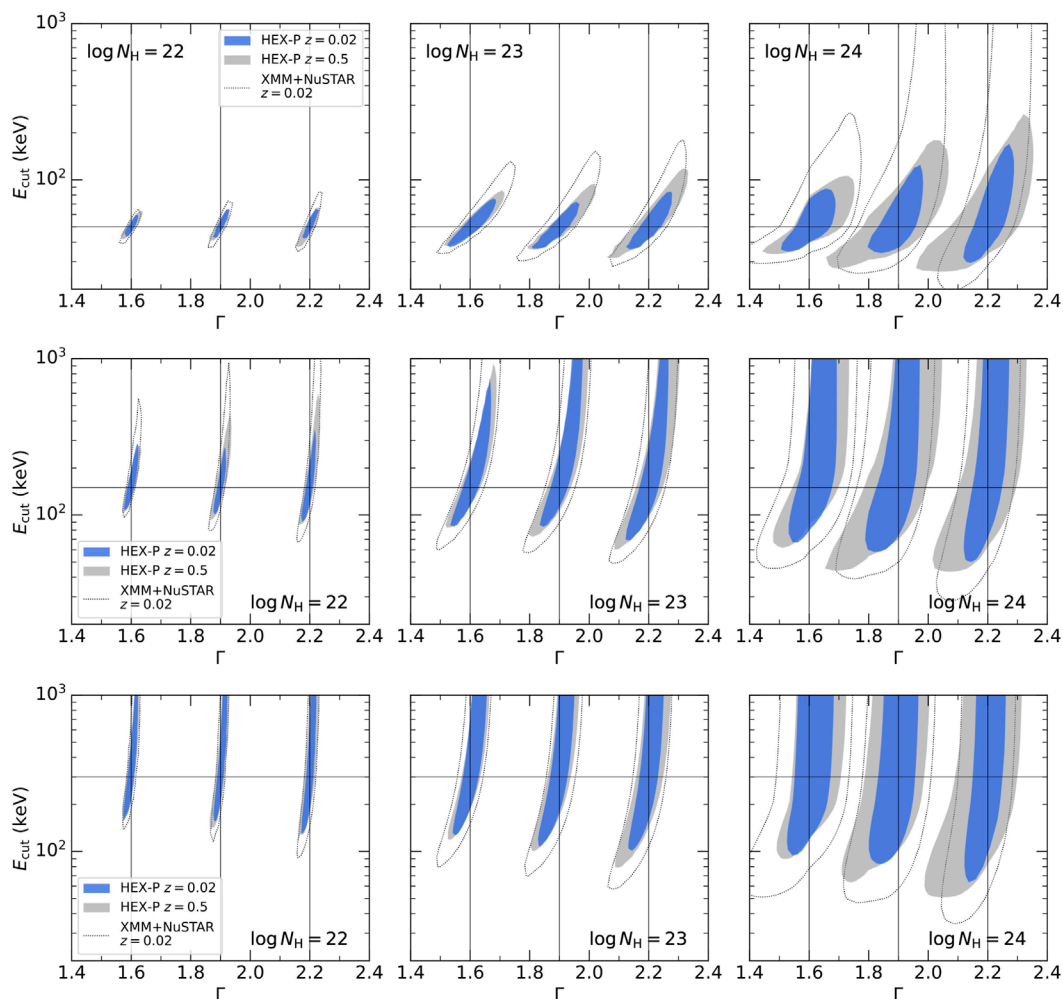
FIGURE 3
$\Gamma - E_{cut}$ contour plots (3σ confidence level) for $z = 0.02$ and 0.5 (blue and grey contours, respectively) assuming $\log\left(N_H/cm^{-2}\right) = [22, 23, 24]$ (left to right), $E_{cut} = 50, 150,$ and 300 *keV* (top to bottom), and simulating a 100-ks *HEX-P* observation. The black dotted contours correspond to the 3σ confidence level constraints for a source at $z = 0.02$ with 30-ks exposure by *XMM-Newton* combined with a 100-ks exposure by *NuSTAR* (including both modules, FPMA and FPMB). Horizontal and vertical lines indicate the input values of Γ and E_{cut}, respectively.

near and above the Compton-thick regime, the measurement of the energy cut-off is degenerate with the assumed obscurer model. Different obscurer geometries have different Compton-scattering behaviour, altering the reprocessed spectrum up to 400 keV (e.g., Buchner et al., 2019; 2021). Thus the obscurer geometry and the energy cut-off are degenerate. Merely assuming an obscurer geometry may bias the energy cut-off measurement. Here, for simplicity, a fixed obscurer model (borus02) was used for generating and modeling the data. The complex task of inferring the true obscurer geometry and the true energy cut-off thus would have to be achieved simultaneously, but this is beyond the scope of this paper. Boorman et al. (in prep.) discusses $HEX - P'$'s ability to infer torus geometries in heavily obscured AGN in more detail.

5 Physics of the corona in intermediate-/high-redshift quasars

The high-energy cutoff in the X-ray spectrum (at tens to hundreds keV) can be directly linked to the properties of the corona. Thanks to *NuSTAR*, whose hard X-ray sensitivity is orders of magnitude better than previous missions, a large sample of AGN were observed with unprecedented data quality at hard X-rays. The majority of the observed sources are AGN with low luminosity ($L_{2-10\,keV} = 10^{42}-10^{44}$ erg s^{-1}; see, e.g., Kamraj et al., 2018; Ricci et al., 2018; Baloković et al., 2020), so they are in a region of the $kT_e - \ell$ plane where a broad range of E_{cut} is allowed within the framework of the runaway pair production hypothesis. This can be seen in the left panel of Figure 4 (we assume here $E_{cut} = 2\,kT_e$, $R_c \sim 10\,r_g$, and coronal luminosity $L_c = L_{0.1-200\,keV} \sim 4 \times L_{2-10\,keV}$). Furthermore, most of these sources are in the nearby Universe ($z < 0.1$, Figure 4, right). Therefore, only lower limits to

their cutoff energy were measured at 90% confidence level due to the limited bandpass in the rest frame of local sources (<80 keV), covered by *NuSTAR*.

On the contrary, high-redshift ($z \geq 1$) radio-quiet quasars (mostly with luminosity $L_{2-10\,keV} > 10^{45}$ erg s^{-1}) are ideal sources to constrain high-energy cutoffs thanks to the limited allowed E_{cut} range on the $kT_e - \ell$ plane (assuming kT_e is indeed limited by runaway pair production; see Figure 4, left) and the cosmological redshifting of E_{cut} to the *NuSTAR* observable band. Therefore, they constitute a promising sample to constrain the AGN coronal properties at high luminosity and test the runaway pair production theory. So far, only three $z > 1$ quasars were observed with *NuSTAR* and had their high-energy cutoffs constrained (Lanzuisi et al., 2019; Bertola et al., 2022; Figure 4, right). All three quasars (with $L_{2-10\,keV} > 3 \times 10^{45}$ erg s^{-1}) were found below the critical line on the $kT_e - \ell$ plane as per pair-production models expectations, though note the large uncertainties for two of the sources which leave ambiguous results (Figure 4, left). The well constrained cutoff energies of the three high-z quasars ($\lambda_{Edd} > 0.1$) were 1.5–2.5 times lower than the 160 keV measured by Ricci et al. (2018) for sources with high Eddington ratio. Therefore, observing high-redshift quasars, where the coronal properties could be well constrained, is crucial to study the possible evolution of the corona with the accretion parameters such as the accretion rate and the SMBH mass.

Despite the recent progress in constraining the coronal properties of high-redshift, high-luminosity quasars, the observations are extremely time-consuming. A total of ~375 ks *NuSTAR* and 150 ks XMM observations were spent on the above three sources. The long exposures required in these observations lead to a strong limitation in constraining AGN coronal properties statistically.
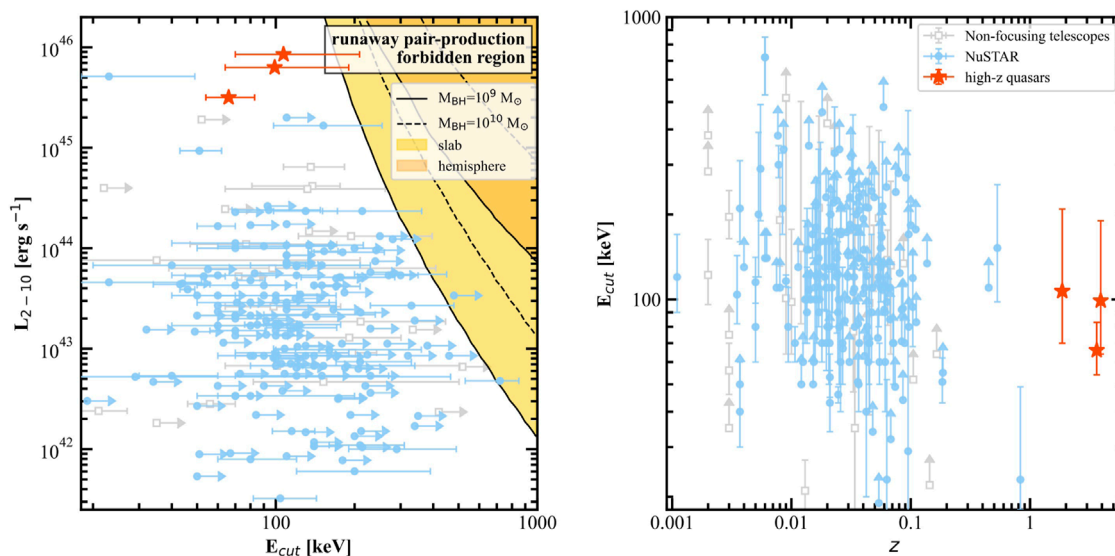
FIGURE 4
High-energy cutoff of AGN as a function of 2−10 keV luminosity (left) and redshift (right) by *NuSTAR* (light blue circles) and non-focusing telescopes (gray squares), based on Bertola et al. (2022). The pair-production forbidden regions assuming different coronal geometries are plotted in orange (hemisphere) and yellow (slab). So far, E_{cut} was only measured in three quasars at $z > 1$ (red stars). E_{cut} is not constrained for most of the low-redshift and low-luminosity AGN.
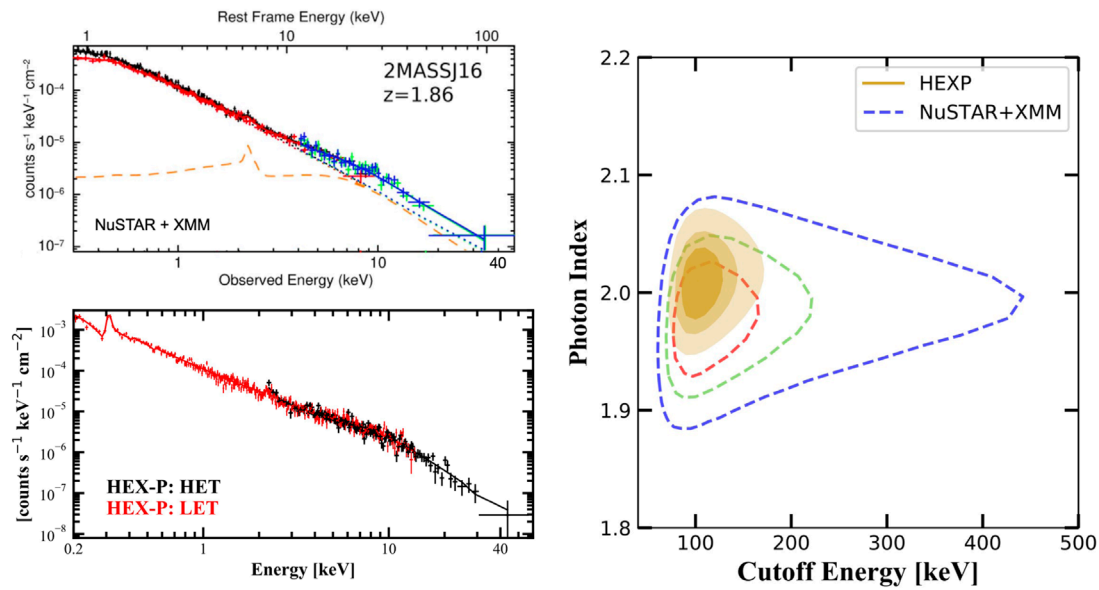
FIGURE 5
Left, upper panel: 140 ks *NuSTAR* (blue) and 69 ks *XMM-Newton* (red) spectra of 2MASS J1614346 + 470,420 at *z* 1.86 (adapted from Lanzuisi et al., 2019). *Left, lower panel:* 140 ks *HEX-P* simulation of the same quasar (HET in black, LET in red). *Right:* contours of E_{cut} and photon index of the *NuSTAR* + *XMM-Newton* observations (red, green, and blue correspond to 68%, 90%, and 99% confidence level, respectively) and *HEX-P* simulations (dark yellow, yellow, and light yellow correspond to 68%, 90%, and 99% confidence level, respectively).

HEX-P, with larger effective area, lower background, and broad band coverage, is well suited to efficiently study the coronal properties of high-redshift, high-luminosity quasars. We compare the 140 ks *NuSTAR*+ 69 ks *XMM-Newton* observation of 2MASS J1614346 + 470,420 ($z = 1.86$) from Lanzuisi et al. (2019) to a simulated 140 ks *HEX-P* observation in Figure 5. Note that L1 orbit of *HEX-P* implies that the *HEX-P* observation would take half the total observatory time compared to the *NuSTAR* observation, since *NuSTAR* is in low-Earth orbit and does not re-point during Earth occultations. The 90% confidence level constraints on E_{cut} are 106^{+100}_{-40} keV from *NuSTAR* + *XMM-Newton* and 103^{+30}_{-20} keV from the simulated *HEX-P* spectra, implying significantly improved constraints on E_{cut} by *HEX-P* in the same exposure time and half the clock time. The high-energy cutoff and the photon index contours (at 68%, 90%, and 99% confidence levels) derived from *NuSTAR* + *XMM-Newton* and simulated *HEX-P* spectra are plotted in the right panel of Figure 5. The contours show that *HEX-P* can constrain E_{cut} at high confidence.

HEX-P will not only provide better constraints on AGN coronal properties but it will also efficiently probe AGN coronæ in a large sample of high-redshift, high-luminosity quasars. We demonstrate the constraining power of *HEX-P* for coronal cutoff energy measurements of intermediate-/high-redshift, high-luminosity quasars. We simulated nine *HEX-P* observations of quasars with 50 ks exposures assuming an input 2–10 keV flux of $F_{2-10\,keV} = 10^{-12}$ erg s^{-1} cm^{-2}. We note that cosmic X-ray background population synthesis models predict ~ 200 quasars at $z > 1$ with such flux level (see, e.g., Gilli et al., 2007). The input redshifts range goes from $z = 0.65$ to $z = 4.5$, so that their 2–10 keV intrinsic luminosity range over $\log(L_{2-10\,keV}/\mathrm{erg}\ s^{-1}) = 45.25$–47.25.

We simulated source spectra assuming a cutoff power law with a Galactic absorption of 10^{20} cm^{-2} and photon index of $\Gamma = 1.90$. We simulated three different high-energy cutoffs, $E_{cut} = 50$, 100, and 200 keV, to explore the parameter space. Assuming the same supermassive black hole mass, $\log(M_{BH}/M_\odot) = 9.2$ and a 2–10 keV luminosity to bolometric luminosity conversion factor of 20 (e.g., Vasudevan and Fabian, 2007; Lusso et al., 2012), the Eddington ratios of the sample range over $\lambda_{Edd} = 0.2$–20.

Figure 6 shows the $E_{cut} - \Gamma$ contours measured from the simulated spectra of the quasars with different redshifts and different high-energy cutoffs. The best-fit high-energy cutoffs of each simulated spectrum with its 90% confidence level uncertainties are indicated on the upper right corner of each panel. As expected, E_{cut} is better constrained at higher redshift thanks to the cosmological redshifting, given the fact that we conserve the flux ($F_{2-10\,keV} = 10^{-12}$ erg s^{-1} cm^{-2}) of each simulated source at different redshifts. Likewise, sources with $E_{cut} = 50$ keV are better constrained than higher E_{cut} sources at all redshifts due to the band coverage of *HEX-P*. We found that it is difficult to constrain the high-energy cutoff of intermediate redshifts ($z < 1.1$) sources with $E_{cut} = 200$ keV in a 50 ks exposure.

We tested the E_{cut} constrained by *HEX-P* assuming different photon indices ($\Gamma = 1.60$, 1.90, and 2.20) under a few redshifts ($z = 0.85$, 1.40, 2.20, and 3.50) assuming the same flux as above. The results are reported in Table 1. We found that harder photon index provides better constraints on E_{cut} than softer photon index at all redshifts because more high energy photons are obtained for harder photon indices and a given 2–10 keV flux. The differences of the constraints on E_{cut} between softer and harder photon indices are much larger at lower redshifts than at higher redshifts. Nevertheless,
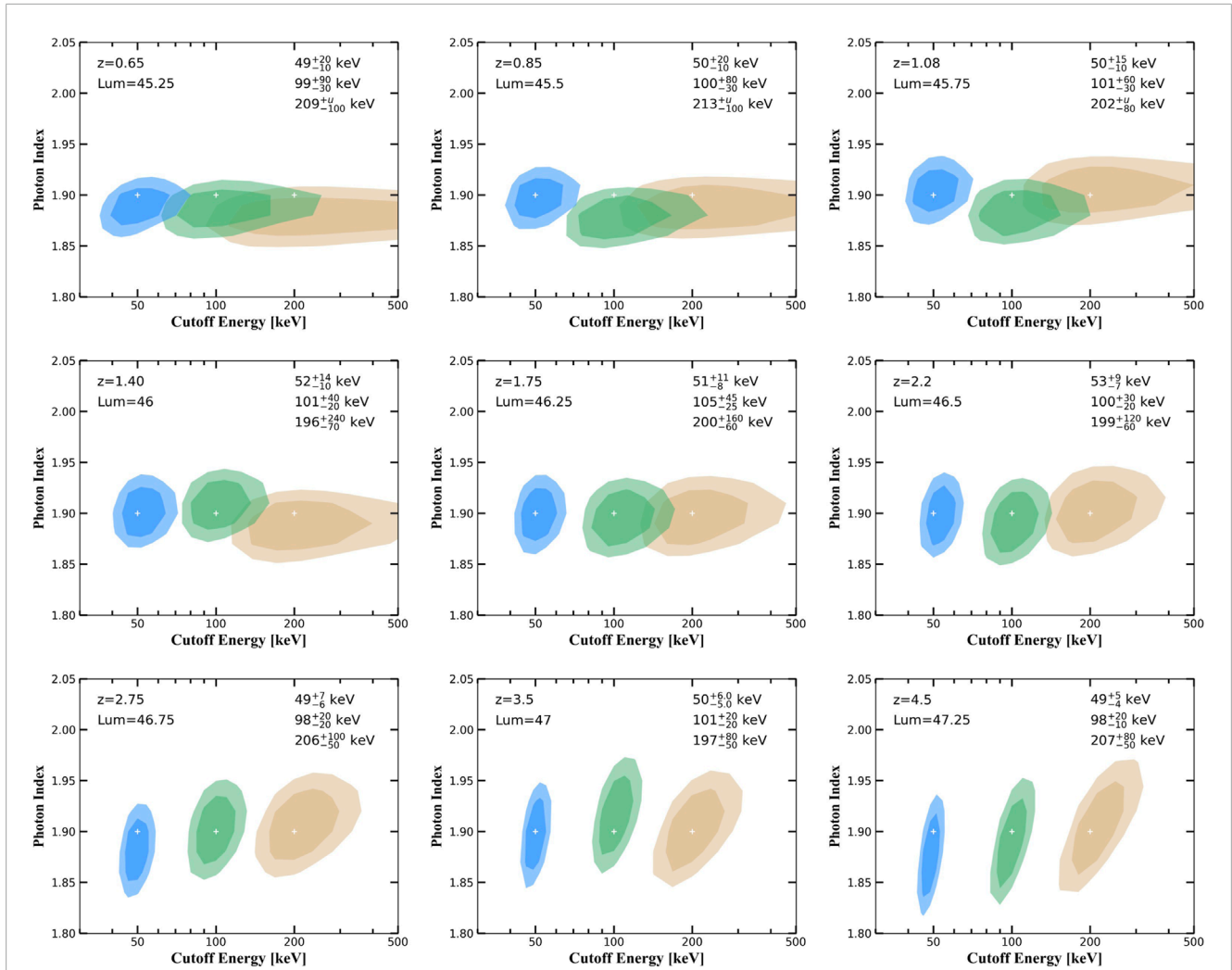
FIGURE 6

$E_{\rm cut} - \Gamma$ contour plots (68% and 90% confidence levels) measured from the simulated spectra of the quasars with different redshifts (0.65 < z < 4.5), assuming an input 2−10 keV flux of 1×10^{-12} erg s^{-1} cm^{-2} and a *HEX-P* exposure of 50 ks We simulated three set of high-energy cutoff for each source, $E_{\rm cut}$ = 50, 100, and 200 keV (blue, green, and yellow). The white crosses indicate the input values. The best-fit value of each spectrum with its 90% confidence level uncertainty is indicated on the upper right corner of each panel.

TABLE 1 Constraints on the high-energy cutoff with different photon indices under different redshifts.

z	Γ = 1.6	Γ = 1.9	Γ = 2.2	Γ = 1.6	Γ = 1.9	Γ = 2.2	Γ = 1.6	Γ = 1.9	Γ = 2.2
	50 keV			100 keV			200 keV		
0.85	51^{+12}_{-9}	50^{+17}_{-10}	51^{+42}_{-15}	100^{+42}_{-24}	100^{+78}_{-31}	95^{+104}_{-34}	205^{+237}_{-74}	213^{+u}_{-96}	213^{+u}_{-117}
1.40	51^{+9}_{-7}	52^{+14}_{-9}	51^{+23}_{-12}	102^{+30}_{-20}	101^{+40}_{-20}	96^{+70}_{-30}	205^{+140}_{-60}	196^{+240}_{-70}	205^{+u}_{-90}
2.20	50^{+6}_{-6}	53^{+9}_{-7}	50^{+11}_{-8}	99^{+23}_{-16}	100^{+30}_{-19}	101^{+39}_{-23}	197^{+80}_{-50}	199^{+120}_{-60}	190^{+175}_{-55}
3.50	50^{+6}_{-5}	50^{+6}_{-5}	51^{+7}_{-6}	99^{+20}_{-15}	101^{+20}_{-15}	101^{+23}_{-17}	197^{+80}_{-45}	197^{+80}_{-45}	197^{+80}_{-45}

HEX-P could constrain the $E_{\rm cut}$ in most circumstances even for the sources with quite soft photon index, $\Gamma = 2.20$.

eROSITA (Predehl et al., 2021) observations will provide an all-sky survey of X-ray sources, which will be the deepest survey in the soft X-rays ever performed. With the ongoing SDSS and DESI surveys, and future *Euclid*, 4MOST, Subaru Prime Focus Spectrograph, and *SPHEREx* spectroscopic surveys, a large number of high-redshift, high-luminosity, radio-quiet AGN are expected

to be discovered prior to the launch of *HEX-P*. The combination of these large surveys should therefore provide a large sample of high-redshift quasars for *HEX-P* coronal physics studies in the next decade.

6 Physics of the corona in transient sources: changing-look/changing-state AGN and tidal disruption events

The growing number of time-domain surveys across the electromagnetic spectrum are revealing extreme variability in the accretion process onto supermassive black holes. These objects break from the standard stochastic variability seen in steadily accreting AGN, and thus provide a unique window into the formation, stability, and heating of the corona.

Changing-look AGN (CLAGN; also often referred to as changing-state AGN) show rapid changes between optical spectral types through either the appearance or disappearance of broad emission lines on timescales of months to years (for a recent review, see Ricci and Trakhtenbrot, 2022). These sources challenge the classic unified model for AGN, whereby the appearance of broad emission lines is solely a function of viewing angle. Instead, the change between optical spectral types is often coupled with an associated increase or decrease in the observed optical and X-ray flux, suggesting that the accretion rate is another key factor in AGN unification (e.g., Elitzur et al., 2014). The driving mechanism behind these changing-look events is still under debate, with theories including state transitions reminiscent of the behavior in black hole binaries (Noda and Done, 2018; Ruan et al., 2019), radiation pressure disk instabilities (Sniegowska et al., 2020), propagating cooling fronts linked to changes in the magnetic torques in the innermost regions of the accretion flow (Ross et al., 2018; Stern et al., 2018), and transient events like tidal disruption events (TDEs; e.g., Merloni et al., 2015; Ricci et al., 2020).

Although CLAGN are still a relatively rare phenomenon with only about 100 such systems known to date, they provide unique insights into the dynamic behavior of the inner accretion flow and unveil physics that is impossible to probe in standard steady-state AGN. One extreme example is evidenced by the recent discovery of the disappearance and recreation of the X-ray corona in 1 ES 1927 + 654. In late 2017, the source underwent one of the fastest changing-look events to date, whereby broad emission lines were caught forming on timescales of months (Trakhtenbrot et al., 2019). Shortly after the start of the changing-look event, X-ray observations of 1 ES 1927 + 654 revealed negligible hard X-ray emission, indicating that the X-ray corona had vanished in this source (Ricci et al., 2020; 2021). The corona began to reappear as the source brightened in the X-ray, although it remained extremely soft compared to standard AGN ($\Gamma \approx 3$–3.5; Ricci et al., 2021; Masterson et al., 2022). Two competing theories have been suggested to explain the behavior in this kind of system: a TDE occurring in an AGN (Ricci et al., 2020), or an inversion in the magnetic flux polarity (Scepi et al., 2021; Laha et al., 2022). Both theories can effectively cut off the energy supply to the corona, leading to its destruction.
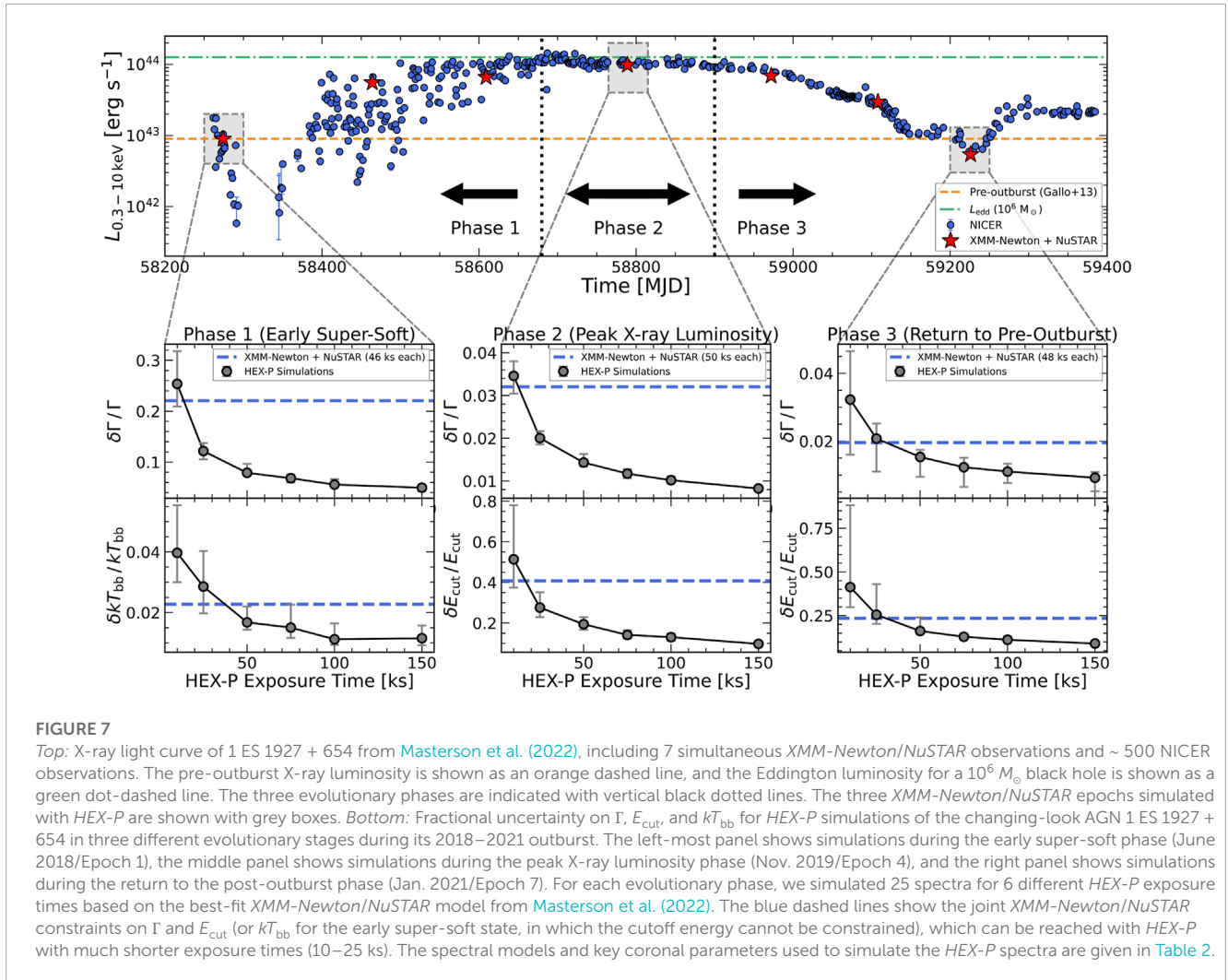
TABLE 2 Spectral models and parameters used in simulations of 1ES 1927 + 654 with *HEX-P*.

Phase	XSPEC model	Γ	E_{cut} (keV)	kT_{bb} (eV)
1	tbabs × ztbabs × (zbbody + zpower + gsmooth (xillverTDE))	3.4	–[†]	88
2	tbabs × ztbabs × (zbbody + zcutoffpl + gsmooth (xillverTDE))	3.6	8.1	205
3	tbabs × ztbabs × (zcutoffpl + relxillCp)	2.3	23.4	–

[†]In this epoch, the source was too soft for proper determination of the cutoff energy, and hence, we used a simple power law to model the spectrum. Note that in the first joint *XMM-Newton*/*NuSTAR*, observation of 1 ES, 1927 + 654, the source was undetected above 3 keV with *XMM-Newton* and was not detected with *NuSTAR*.

As a unique opportunity to witness, for the first time, the formation of the corona in an AGN, there have been extensive X-ray resources used to study this enigmatic outburst of 1ES 1927 + 654. To date, *NICER* has observed the target for more than 1 Ms, and there have been 8 simultaneous *XMM-Newton*/*NuSTAR* monitoring periods, totalling more than 400 ks with each telescope. *NuSTAR* observations have been crucial for disentangling the soft photon index and low cutoff energy as the corona formed, which is not possible with either *XMM-Newton* or *NICER* alone due to their limited bandpasses. However, both *XMM-Newton* and *NICER* have been critical to unlocking information about the inner accretion flow with their soft X-ray spectra, including providing crucial information about rapid variability of the soft X-ray flux and the broad 1 keV line, that was recently linked to reflection from the inner disk (Masterson et al., 2022). To fully understand this system therefore requires a broad bandpass, which is provided by a single observatory in *HEX-P*.

To assess the contributions *HEX-P* can make to our understanding of the corona in CLAGN, we simulated the three different phases in the outburst of 1ES 1927 + 654 as would be seen with the LET and HET on *HEX-P*. For each phase, we simulated *HEX-P* spectra using the best-fitting *XMM-Newton*/*NuSTAR* models from Masterson et al. (2022) with six exposure times ranging from 10 to 150 ks The model used for each phase, along with the key coronal parameters used in the simulations, are given in Table 2. Figure 7 shows the resulting constraints on key coronal parameters Γ and E_{cut} for each evolutionary phase, as well as constraints on kT_{bb} of the dominant thermal component in the early super-soft phase (in which constraints on E_{cut} were not possible given the super-soft nature of the source). We compare these constraints to the ones achieved by 50-ks joint *XMM-Newton*/*NuSTAR* observations, which vary with the changing spectral shape and flux of the source. We find that *HEX-P* can reach similar constraints as from joint *XMM-Newton*/*NuSTAR* observations in a fraction of the exposure time. These simulations show that *HEX-P* could probe the evolution of the cutoff energy and photon index on roughly 10–25 ks timescales, meaning that either the source could be visited relatively frequently to track the evolution over weeks-months timescales, or that a single long stare could be broken into many 10–25 ks segments

FIGURE 7

Top: X-ray light curve of 1 ES 1927 + 654 from Masterson et al. (2022), including 7 simultaneous *XMM-Newton/NuSTAR* observations and ~ 500 NICER observations. The pre-outburst X-ray luminosity is shown as an orange dashed line, and the Eddington luminosity for a $10^6 \, M_\odot$ black hole is shown as a green dot-dashed line. The three evolutionary phases are indicated with vertical black dotted lines. The three *XMM-Newton/NuSTAR* epochs simulated with *HEX-P* are shown with grey boxes. *Bottom:* Fractional uncertainty on Γ, E_{cut}, and kT_{bb} for *HEX-P* simulations of the changing-look AGN 1 ES 1927 + 654 in three different evolutionary stages during its 2018−2021 outburst. The left-most panel shows simulations during the early super-soft phase (June 2018/Epoch 1), the middle panel shows simulations during the peak X-ray luminosity phase (Nov. 2019/Epoch 4), and the right panel shows simulations during the return to the post-outburst phase (Jan. 2021/Epoch 7). For each evolutionary phase, we simulated 25 spectra for 6 different *HEX-P* exposure times based on the best-fit *XMM-Newton/NuSTAR* model from Masterson et al. (2022). The blue dashed lines show the joint *XMM-Newton/NuSTAR* constraints on Γ and E_{cut} (or kT_{bb} for the early super-soft state, in which the cutoff energy cannot be constrained), which can be reached with *HEX-P* with much shorter exposure times (10−25 ks). The spectral models and key coronal parameters used to simulate the *HEX-P* spectra are given in Table 2.

in which the evolution of Γ and E_{cut} could be studied. The X-ray flux of 1ES 1927 + 654 varied by an order of magnitude in timescales as short as 8 h while the corona was in the process of forming (Ricci et al., 2020), which would allow *HEX-P* to provide unprecedented constraints on the evolution of the temperature and compactness of a newly forming corona for the first time. Since the discovery of 1ES 1927 + 654, other sources with similarly dramatic X-ray variability have been discovered (e.g., a repeating TDE discovered by eROSITA, which shows a repetitive creation and collapse of the X-ray corona; Liu et al., 2023).

Moreover, non-jetted TDEs present another opportunity to witness the formation of the corona around SMBHs, and *HEX-P* will play a major role in improving our understanding of various aspects of TDEs. Although detailed simulations go beyond the scope of the current manuscript, we highlight some of these science cases below. The majority of X-ray emitting, non-jetted TDEs show dominant thermal emission, presumably from the accretion disk, but a handful of sources have shown evidence for the formation of a corona in late-time (~ few years after ignition) X-ray observations (e.g., Wevers et al., 2021; Yao et al., 2022). As TDEs are believed to transition from super-to sub-Eddington when the mass fallback rate drops as stellar debris is accreted, they are another powerful probe

of how the corona evolves with changes to the accretion state. A correlation between the Eddington ratio and X-ray spectral state has been already observed in a (small) sample study (Wevers, 2020), with a slope that is remarkably similar to that seen in AGN samples (see, e.g., Lusso and Risaliti, 2016). *HEX-P* studies will enable constraints on the formation and evolution of the corona while *simultaneously* constraining the high-energy cutoff energy over a wide range of accretion rates in individual SMBHs. This direct probe the disk-corona connection during different accretion states will allow for a comparison to state transitions in black hole binaries (Remillard and McClintock, 2006) and serve as a test of the scale-invariant nature of accretion.

X-ray observations of TDEs can also provide independent estimates of SMBH masses and spins, which are otherwise difficult to probe in dormant SMBHs. Detailed X-ray spectral modelling of the thermal continuum in TDEs can provide constraints on the mass and the spin of the central black hole (e.g., Wen et al., 2020). With its wide energy coverage, *HEX-P* will be able to advance this technique by mitigating the inherent uncertainties and bias introduced by the presence of an X-ray corona. Furthermore, X-ray variability is also a powerful probe of SMBH properties. In particular, the SMBH spin can be estimated through the detection

of X-ray quasi-periodic oscillations and/or disk precession (e.g., Pasham et al., 2019), and the SMBH mass can be measured with the break frequency of the power spectral distribution (PSD) (McHardy et al., 2006). In TDEs, the PSD behaviour has been shown to change with Eddington ratio (Saxton et al., 2012; Wevers et al., 2021), and hence can provide an independent estimate of the SMBH mass in TDEs. Additionally, if TDEs form a corona at late times when the accretion rate has dropped and the disk is geometrically thin, then the Fe Kα line can be used to constrain the corona geometry and SMBH spin (e.g., Yao et al., 2022). Thanks to its broad energy coverage, high throughput, low background, and L1 orbit permitting long observations, *HEX-P* will be able to improve our understanding of TDEs using all of these techniques. This will provide several independent mass and spin measurements of quiescent black holes, which would add invaluable information to constrain the demographics of quiescent low mass SMBHs ($<10^7 M_\odot$) that is not readily available through other means.

7 Coronal geometry

One of the key advances in recent years has been the ability to measure the location, geometry and structure of the corona using X-ray reflection and reverberation from the inner regions of the accretion disk. Determining the structure of the corona in this way places important constraints on the mechanism by which the corona is formed and energized by the accretion flow, for example, distinguishing between a corona that is formed in a jet or failed jet, from a corona that is formed over the surface of the inner accretion disk.

In addition to understanding the physics of the corona itself, measurements of the location and geometry of the corona are important to validate assumptions that underpin the use of X-ray reflection spectroscopy to measure fundamental properties of the black hole, such as its spin (Fabian et al., 1989; Dauser et al., 2013; Risaliti et al., 2013; Mallick et al., 2022). One of the predominant techniques employed to measure black hole spin is based upon identifying the innermost radius of the accretion disk (assumed to coincide with the innermost stable circular orbit, ISCO) from the extremal redshift detected in emission lines (namely, the iron K line) within the reflection spectrum (see Brenneman and Reynolds, 2006; Reynolds, 2021; Piotrowska et al., 2023). The intensity of the reflection and the line emission profile, however, depends upon the geometry of the corona, which provides the primary source of illumination. Typically, either a point source (or "lamppost") is assumed, or a phenomenological power law is used to model the emissivity profile of the disk (i.e., the intensity of the reflected flux as a function of radius). If the model corona or power law over-predicts reflection from the inner disk, the corona is at a greater height or is more extended than assumed in the model, and it is possible that the spin of the black hole is underestimated (Fabian et al., 2014). First-hand measurements of the location and geometry of the corona reduce this systematic uncertainty and the degeneracy that arises between extended coronæ and low spins.

HEX-P will enable measurements of the location, geometry and structure of the corona via both broadband X-ray spectroscopy and timing. The former is based upon direct measurement of the emissivity profile of the disk from the reflection observed in time-averaged X-ray spectra. The latter technique utilizes the light travel time between the corona and disk as variations in the luminosity of the primary X-ray emission reverberate off of the accretion disk. In addition, further constrains on the geometry of the X-ray corona are available from X-ray polarisation measurements, which can distinguish between X-ray emission from a compact corona, a corona associated with a jet, or an extended slab-like corona extending over the inner accretion disk (see, e.g., Marinucci et al., 2022a; Gianolli et al., 2023; Tagliacozzo et al., 2023; Ursini et al., 2023).

7.1 Measurements of the corona via X-ray spectroscopy

The emissivity profile of the disk is encoded in the profile of the relativistically broadened emission lines. The emission line we observe is the line emission integrated over the entire disk, and is comprised of photons experiencing different Doppler shifts and gravitational redshifts, which vary as a function of position on the disk. This means that it is possible to fit the observed line profile as the sum of contributions from different radii on the disk, and the relative contribution of the line model from each radius provides a measurement of the emissivity profile (Wilkins and Fabian, 2011). The measured profile can then be compared to theoretical predictions for the illumination of the disk by coronæ with different geometries and at different locations (Wilkins and Fabian, 2012; Dauser et al., 2013). Alternatively, a geometry can be assumed for the corona (usually a point source, or lamppost), and a model can be fit directly to full reflection spectrum to make a measurement of the coronal parameters; namely, the height of the corona for the lamppost (Dauser et al., 2016). The emissivity profile of the disk is sensitive to the coronal height in the case of a lamppost geometry, or to the radial extent of the corona if it were extended over the surface of the disk (Wilkins and Fabian, 2012).

A further measurement of the corona comes from the ratio of the reflected flux to the flux of the continuum that is observed directly from the corona, referred to as the reflection fraction (Wilkins and Gallo, 2015; Dauser et al., 2016). In the case of an isotropically emitting point source above an infinite accretion disk in a flat spacetime, we expect a reflection fraction $R_f = 1$, since exactly half of the emission from the corona is emitted downwards to illuminate the disk, and half is emitted upwards to escape to be observed as the continuum. Light bending around the black hole causes a greater fraction of the rays to be focused towards the inner accretion disk, enhancing the reflection fraction relative to the continuum when the corona is confined to a more compact region of space, closer to the black hole, providing another probe of the compactness of the corona (Fabian et al., 2012; Parker et al., 2014; Walton et al., 2021). On the other hand, the reflection fraction can be reduced below unity if it is outflowing at a mildly relativistic velocity (for example, if the corona is part of a jet or failed jet). In this case, the coronal emission is relativistically beamed away from the accretion disk, enhancing the fraction of rays that are able to escape to be observed as part of the continuum (Beloborodov, 1999; Gonzalez et al., 2017). The broad bandpass of *HEX-P* is vital to obtain an accurate measurement of the total reflection fraction.

In addition, by combining measurements of the reflection fraction with measurements of the relativistically broadened iron K line and the associated reverberation time lags, *HEX-P* will be able to obtain measurements of the location, the geometry, and the motion of the X-ray emitting coronæ around black holes.

7.2 X-ray reverberation from the inner accretion disk

The measurement of X-ray reverberation time lags adds a further dimension to the picture of the corona. The reflection and line emission from the accretion disk responds to short-timescale changes in luminosity of the primary X-ray emission from the corona. There is, however, a time delay between variations in the continuum and the correlated variations in the reflection due to the additional light travel time between the corona and disk (Fabian et al., 2009; Uttley et al., 2014). In the sample of AGN in which reverberation has been detected, the measured time delays are short and correspond to the light crossing time across distances of between approximately one and ten gravitational radii (this is approximately equal to the radial co-ordinate of the event horizon of a maximally spinning black hole). Such short time delays indicate that the corona must be compact and confined to a small region of space close to the black hole and innermost accretion flow (e.g., De Marco et al., 2013; Kara et al., 2016; Mallick et al., 2021). The reverberation time scale is primarily sensitive to the scale height of the corona above the disk (Wilkins and Fabian, 2013; Cackett et al., 2014). In recent years, there have also been advances in simultaneously modelling the X-ray spectrum and time lag measurements under the assumption of a point-like corona, using models such as RELTRANS (Ingram et al., 2019). With simultaneous fitting, it is possible to obtain simultaneous constraints on both the height of the corona and the mass of the black hole (e.g., Mastroserio et al., 2020).

HEX-P measurements of X-ray reflection and reverberation were simulated for nearby AGN, typical of those in which reverberation from the inner disk has been detected (e.g., Kara et al., 2015; 2016; Mallick et al., 2021). These are predominantly narrow line Seyfert 1 (NLS1) AGN (Gallo, 2006), which show strong, relativistically broadened iron K lines from the inner accretion disk and a high degree of short-timescale variability in their X-ray light curves (see, e.g., Gallo, 2018, for a review). The observations were simulated from a full spectral-timing reverberation model, which begins with general relativistic ray tracing calculations between a point-like corona, the accretion disk, and the observer, using the CUDAKERR code of Wilkins and Fabian (2012) and Wilkins et al. (2016). These ray tracing calculations self-consistently predict the illumination of the disk by the corona, and the energy shifts and time delays of the observed reflection and reverberation in the form of the impulse response function (Reynolds and Begelman, 1997; Cackett et al., 2014; Uttley et al., 2014). The response function is then convolved with the XILLVER model for the reflection spectrum produced in the rest frame of the material in the disk (García et al., 2013) to predict the full spectral-timing response. The simulations generate the observed X-ray spectrum (including the instrumental background), and the light curves that would be observed in different energy bands, folded through the response functions of the *HEX-P* telescopes and detectors, allowing measurements of the spectrum and time lags to be conducted as they would be for real observations.

The left panel of Figure 8 shows the simulated broadband X-ray spectrum and time lag spectrum for a typical Seyfert-like AGN displaying X-ray reverberation for a deep 500 ks observation with *HEX-P*. Reverberation is simulated around a maximally spinning ($a = 0.998$) black hole with a mass of $10^7\,M_\odot$ at a redshift of $z = 0.025$. The observed flux is equivalent to accretion at 0.3 times the Eddington limit, and 5 per cent of the total bolometric luminosity is produced by the corona. Parameters of the corona and accretion disk are selected to be representative of the typical reflection spectra observed in nearby AGN (e.g., Jiang et al., 2018; Mallick et al., 2018). The X-ray spectrum shows the characteristic features of X-ray reflection from the inner disk: a) the iron K line around 6.4 keV, with an extended redshifted wing comprised of the line photons emitted from the innermost radii of the accretion disk; b) the Compton hump around 20 keV; and c) a soft excess formed as soft X-ray lines are blended together by relativistic broadening. The ability to simultaneously measure the soft X-ray band, the broad iron K line, and the Compton hump will allow *HEX-P* observations to unambiguously separate reflection from the accretion disk from other spectral components (e.g., Walton et al., 2014).

The characteristic form of the reflection spectrum is also evident in the time lag spectrum. The energy bands dominated by reprocessed emission from the disk, namely, the soft excess, the iron K line, and the Compton hump, are seen to respond to variations at later times than the energy bands dominated by continuum emission observed directly from the corona (1.5–3 keV and 8–10 keV). The broad bandpass covered by the combination of the LET and HET on *HEX-P*, combined with the available effective area, mean that *HEX-P* is sensitive to reverberation time lags across the full range of the reflection spectrum. It will be possible to measure the differential time lag between the redshifted wing of the iron K line, which arises from the inner disk, closer to the black hole and corona, and the 6.4 keV core of the iron K line from larger radii. The difference in time lag between the inner and outer disk is a sensitive probe of the structure of the corona (Wilkins et al., 2016). *HEX-P* will be able to routinely measure the reverberation time delays associated with the Compton hump, only hints of which have so far appeared in *NuSTAR* observations (Kara et al., 2015; Zoghbi et al., 2017).

7.3 Simulation of *HEX-P* reverberation measurements

To demonstrate the sensitivity of *HEX-P* to X-ray reverberation and its effectiveness in measuring the structure of the corona across the supermassive black hole mass spectrum, iron K reverberation measurements were simulated for a sample representative of the 25 brightest nearby AGN in the BASS catalog, each observed for 300 ks with *HEX-P*. For each of these simulated AGN, the mass, bolometric luminosity, redshift and absorption were drawn from the BASS catalog (Koss et al., 2022). The remaining parameters of the black hole, accretion disk and corona were drawn randomly from distributions representing the reverberation sample (since
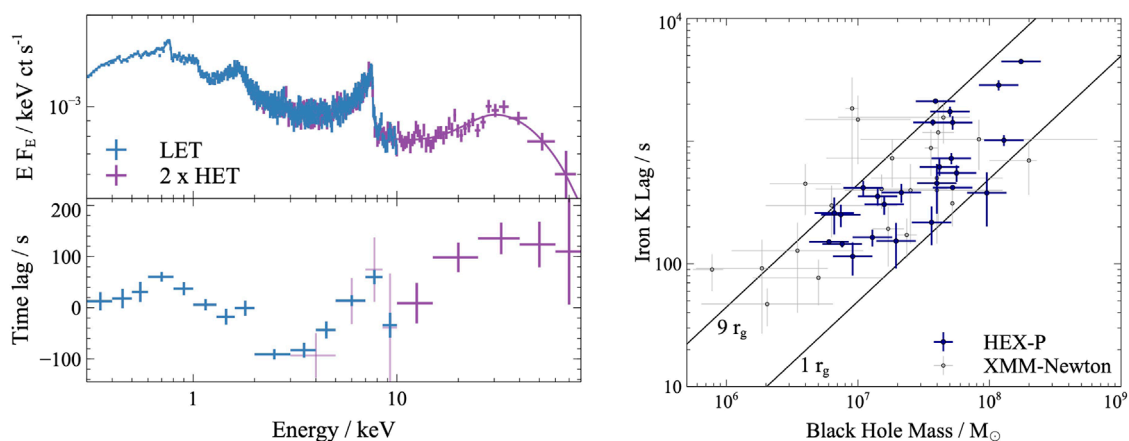
FIGURE 8

Left: Simulated 500 ks *HEX-P* observation of a typical nearby AGN, showing X-ray reflection and reverberation from the inner accretion disk. The top panel shows the simulated X-ray spectra obtained with the LET and HET. The relativistically broadened iron K line (around 6.4 keV) and Compton hump (around 25 kev) that are characteristic of reflection from the inner disk are clearly visible. The bottom panel shows the measured time lag vs. energy spectrum, which shows the relative time at which different energy bands respond as variations in the continuum emission reverberate off the disk. The energy bands dominated by reflection from the disk (the soft X-ray excess, below 1 keV, the broad iron line, and the Compton hump) lag behind the bands dominated by the primary continuum observed directly from the corona. This time delay arises from the additional light travel time between the corona and accretion disk, and is a sensitive probe of the location and geometry of the corona. *Right:* Simulated iron K reverberation lag measurements as a function of black hole mass for a simulated sample of AGN based upon the BASS sample. For each simulated AGN, the mass, luminosity, and redshift are representative of the real sample, and the remaining parameters of the black hole, disk, and corona are drawn from random distributions. Each of the simulated AGN is observed for 300 ks with *HEX-P*. Error bars on the black hole mass values assume mass measurements can be made via optical reverberation, and correspond to a representative uncertainty of 0.15 dex.

detailed spectral analyses are not available for all of the BASS AGN[4]). The reverberation measurement was simulated as described above, predicting the time lag vs. Fourier frequency that would be measured by *HEX-P* between the continuum-dominated 1.2–4 keV band and the 4–7 keV iron K band. We select the frequency bin with the highest signal-to-noise (i.e., the ratio between the lag and the lag uncertainty) as the representative iron K lag value.

The right panel of Figure 8 shows the simulated iron K reverberation lag measurements as a function of black hole mass for the BASS AGN sample, compared to the equivalent measurements made in a sample of nearby Seyfert galaxies using *XMM-Newton* (Kara et al., 2016). *HEX-P* will significantly detect reverberation in the iron K line and trace the relationship between the reverberation time lag and the mass of the black hole. From these simulations, we expect that *HEX-P* will be able to measure iron K lags in a sample of AGN between redshifts of $z = 0.005$ and $z = 0.14$, with bolometric luminosities between 3×10^{43} and 10^{46} erg s^{-1} (assuming 5 per cent of this is emitted across the broad 0.1–100 keV X-ray band). The simulations show that iron K lags will be measured to high precision, with a median uncertainty of 13 per cent across the sample from 300 ks observations. Longer observations of around 500 ks will enable an additional reverberation measurement to be made in the Compton hump to constrain the broadband time lag

spectrum, to which more detailed reverberation models can be fit (as demonstrated in the left panel).[5]

Notably, *HEX-P* will also be able to detect reverberation around the most massive black holes in the sample ($\gtrsim 10^8 M_\odot$), where the reverberation timescale is expected to be longer (if it scales simply with the gravitational radius around the black hole). The ability to measure long-timescale lags using common Fourier techniques (Uttley et al., 2014) is limited by the duration of continuous light curves that can be obtained. The highly elliptical orbit of *XMM-Newton* limits individual observations, and hence individual light curve segments, to ~125 ks. At its L1 orbit, *HEX-P* will be able to perform much longer continuous exposures (in principle up to 12 days), greatly lengthening the timescales that can be probed. Combined with the fact that the highest mass AGN are some of the brightest in the BASS sample, iron K reverberation is expected to be detected at high significance.

8 Black hole X-ray binary coronæ

This work has focused on coronæ in the vicinity of extragalactic SMBHs, primarily observed through hard X-ray emission from AGN. However, Galactic black hole X-ray binaries (BHXRBs) can

---

4 The probability distributions from which the parameter values are drawn were chosen to be consistent with the range of parameter values from the sub-set of the BASS AGN sample for which spectroscopic measurements are available, detailed at www.bass-survey.com and in Ricci et al. (2017).

5 In Figure 8, the error bars on mass measurements assume that the mass can be measured by optical reverberation. We assume a representative uncertainty of 0.15 dex on the black hole mass, the median of those obtained by reverberation measurements in the Black Hole Mass Database (Bentz and Katz, 2015).

be viewed broadly as scaled-down versions of AGN, particularly from the point of view of the compact regions close to the BH (Falcke et al., 2004; Körding et al., 2006; McHardy et al., 2006; Walton et al., 2012). Many BHXRBs–those with low-mass companion stars–are transient sources, undergoing outbursts lasting weeks to years, during which they display a full repertoire of accretion states and regularly exceed X-ray fluxes of 1 Crab (see, e.g., Remillard and McClintock, 2006; Tetarenko et al., 2016). Given the broad dynamical range one can probe via studies of BHXRBs, much can be learned about the long-term behaviour and evolution of AGN through observations possible on human timescales. In addition, the high fluxes of outbursting BHXRBs allow for characterization of the broadband X-ray continuum with exquisite detail, making them a primary target for *HEX-P*.

As briefly discussed in Section 3, today's X-ray observatories already allow us to probe the coronal temperatures of BHXRBs as they decrease with increasing source flux (Buisson et al., 2019; Cangemi et al., 2021; Zdziarski et al., 2021), and these measurements have contributed greatly to our understanding of BH coronæ. However, degeneracies remain in the broadband X-ray continuum emission and geometry of BHXRB coronæ, as well as the AGN ones, and this has been a hindrance to reflection studies aimed at characterizing the inner accretion flow and measuring BH spin. With its broadband coverage, large collecting area, and high energy sensitivity, *HEX-P* will: (i) break degeneracies in the geometry of the irradiating corona intrinsic to reflection models; and (ii) measure deviations from purely thermal Comptonization models, allowing explicit constraints on the non-thermal fraction of BHXRB coronæ. The broadband spectral coverage of *HEX-P* in the 0.2–80 keV range, combined with its high-energy sensitivity (owing to low X-ray background) will be especially powerful in constraining the weaker power law emission in BHXRB soft states, advancing coronal constraints spanning orders of magnitude in luminosity and across the spectral states. We refer the reader to Connors et al. (2023) for a full description of *HEX-P* simulations of BHXRB coronæ.

9 Discussion and conclusion

In this paper, we show the advances that *HEX-P* will make in understanding the physics of the X-ray corona in different types of AGN, ranging from local Seyferts to quasars at cosmological redshifts. The broad passband, large effective area, low background, and the ability to have continuous long exposures will enable addressing many open questions regarding the physics of the X-ray corona in AGN. *HEX-P* will allow an accurate estimate of the continuum emission spectrum of the corona by measuring the photon index and the high-energy cutoff. Assuming a certain geometry, these parameters can then be mapped into optical depth and electron temperature within the framework of Comptonization (see, e.g., Middei et al., 2019). We demonstrate how *HEX-P* will improve our understanding of the electron distribution in AGN coronæ, measure coronal properties of obscured sources, and extend these analyses to $z \geq 1$. Furthermore, we show that *HEX-P* will track variations of bright transient events such as CLAGN and TDEs on timescales of a few hours. *HEX-P* will allow us to study the properties of the X-ray corona and probe the innermost regions of

the accretion disk via reverberation mapping. This will be crucial for understanding how the corona interacts with the accretion disk, studying disk reflection and consequently measure the BH spin in AGN over a broad range of mass and luminosity, and probing AGN feedback (see Piotrowska et al., 2023). Furthermore, *HEX-P* will allow a detailed study of obscuration in AGN and identify the fraction of Compton-thick AGN in deep surveys (see Boorman et al., 2023; Civano et al., 2023). All this will help achieving a more complete picture of how SMBHs grow and evolve across cosmic time, and the role they play in galaxy evolution.

Simultaneous observations with LET and HET, covering the 0.2–80 keV range, will allow an accurate measurement of E_{cut} up to ~1 MeV in bright sources where ionized disk reflection is important. This has been discussed in detail by García et al. (2015) who showed that the soft part of the reflection spectrum, rich in fluorescent lines and atomic features, depends strongly on the properties of the corona, illuminating the accretion disk. García et al. (2015) demonstrated this in the case of joint *NuSTAR* and *Suzaku* spectra. Here, we revisit the analysis presented by those authors for *HEX-P*. We consider a simple spectrum comprised of neutral Galactic absorption (TBabs; Wilms et al., 2000) and a power law plus ionized reflection (relxill; Dauser et al., 2013; García et al., 2014). In XSPEC parlance, the model is written as: M*odel = TBabs × relxill*. We assume a Galactic absorption $N_{\mathrm{H}} = 5 \times 10^{20}$ cm^{-2}. As for the reflection component, we assume a photon index $\Gamma = 2$, a black hole spin $a^{\star} = 0.998$, a disk ionization parameter $\log(\xi/\mathrm{erg} \; cm \; s^{-1}) = 1.5$, an inclination $i = 45°$, a disk emissivity index $q = 3$, and an iron abundance equal to the solar value. García et al. (2015) used similar parameters except for the reflection fraction which they assumed to be $R_f = 3$. This enhances the reflection features in the spectrum. We choose a more conservative value of $R_f = 1$. We then simulate 100-ks observations of *HEX-P* for E_{cut} ranging between 50 keV and 1 MeV for 2–10 keV flux levels of 1 mCrab, 10 mCrab, 100 mCrab, and 500 mCrab. These simulations are intended to represent a wide range of Galactic and extragalactic accreting black holes. We fit the simulated spectra using only the HET and by using both LET and HET simultaneously. Similarly to García et al. (2015), we find that *HEX-P* will allow us to accurately estimate E_{cut} up to ~1 MeV for bright sources (Figure 9). In addition, we also find that the inclusion of LET significantly reduces the uncertainty on E_{cut}. We note that these results assume that the soft X-ray excess is in totality caused by the ionized relativistic reflection from the inner parts of the disk. In fact, the nature of this excess is still a matter of debate as it has been suggested that it could also be caused by the presence of a warm optically thick corona (e.g., Petrucci et al., 2018; 2020). Studying the effect of such model on the properties of the hot corona is beyond the scope of this paper.

9.1 Synergies with other facilities

We have demonstrated the power of *HEX-P* as a stand-alone instrument to advance our understanding of the physics of X-ray coronæ in accreting black holes. However, simultaneous broadband X-ray and multi-wavelength coverage will provide a more comprehensive physical picture of accretion onto these objects.
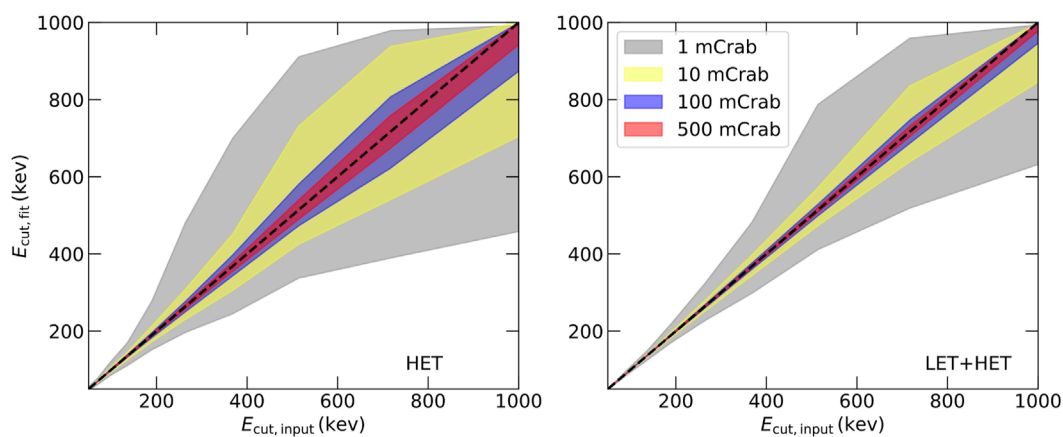
FIGURE 9
Results of fitting *HEX-P* simulations assuming relativistic reflection, by employing only HET (left) and by adding the soft X-rays LET + HET (right). The grey, yellow, blue, and red areas correspond to the 90% confidence level on estimating E_{cut} for observed flux levels of 1 mCrab, 10 mCrab, 100 mCrab, and 500 mCrab, respectively.

HEX-P will play an instrumental role in such studies thanks to its broad passband and high energy sensitivity as demonstrated throughout this paper. The ability to probe the emission from the X-ray corona for a variety of sources with a wide range of mass, luminosity, distance, and variability timescales will make *HEX-P* an essential tool to provide a comprehensive understanding of the behavior and physics of AGN coronæ, which is the dominant source of X-rays in the universe.

For example, the recent advancements made by *IXPE*, observing X-ray polarization in AGN for the first time, required a full characterization of the broadband X-ray spectrum. This has been ensured via simultaneous observations with *XMM-Newton*, *NuSTAR*, and *Chandra*. *HEX-P* will provide equivalent energy coverage to the combination of *XMM-Newton*/*Chandra* and *NuSTAR*, with significant improvements to the high energy sensitivity. *HEX-P* will be an essential complementary observatory to future X-ray polarization missions such as the *X-ray Polarization Probe* (XPP; Krawczynski et al., 2019; Jahoda et al., 2019) and the *enhanced X-ray Timing and Polarimetry* mission (eXTP; Zhang S. et al., 2019).

As mentioned earlier, a correlation between the hard X-ray emission and mm-band continuum has been observed in various samples of AGN (see, e.g., Behar et al., 2018; Kawamuro et al., 2022; Ricci et al., 2023). *HEX-P* will accurately measure the optical depth and temperature of the X-ray corona, as well as determine the fraction of non-thermal electrons producing the X-ray emission for a large sample of AGN. In coordination with ALMA and similar facilities, these parameters can then be used to model the continuum emission in the mm-band and probe the magnetic field powering the corona. *HEX-P* will also complement observations with the Square Kilometer Array and the next-generation of cosmic microwave background experiments (e.g., CMB-S4; Carlstrom et al., 2019; Abazajian et al., 2022).

Moreover, *HEX-P* will play a crucial part in connecting soft X-ray and soft gamma-ray (i.e., up to a few MeV) observations of BHXRBs. In particular, a primary science goal of the *Compton*

Spectrometer and Imager (*COSI*; Tomsick et al., 2019), scheduled for launch in 2027 as a NASA Small Explorer (SMEX) mission, is to characterize the Galactic 511 keV positron annihilation line and the gamma-ray polarization of compact objects. *COSI* will be able to detect a broadened and redshifted pair line from pair-dominated coronæ. The broadband X-ray coverage of *HEX-P* will help constrain the continuum coronal emission, which will be important for modeling the higher energy emission and polarization measurements provided by *COSI*. *HEX-P* will also play a major role in constraining the X-ray emission from gamma-ray emitting AGN detected by *COSI* (see Marcotulli et al., 2023), which will probe the connection between the accretion disk and jets (Ajello et al., 2019), shedding yet more light on the nature of the X-ray corona.

Recent systematic studies of the optical night sky, such as All Sky Automated Survey for Super Novæ (ASASSN; Shappee et al., 2014), the Asteroid Terrestrial-impact Last Alert System (ATLAS; Tonry et al., 2018), and the Zwicky Transient Facility (ZTF; Bellm, 2014; Graham et al., 2019), are providing large numbers of Galactic and extragalactic transients, which are often associated with accretion onto compact objects. The discovery rate of nuclear transients with dramatic X-ray variability, similar to 1ES 1927 + 654, is expected to increase significantly in the next decade with the continued advance of large-scale, time-domain surveys in the optical (e.g., photometry from the Vera Rubin Observatory, spectroscopy from SDSS-V) and UV (e.g., *ULTRASAT*; Sagiv et al., 2014). Therefore, *HEX-P* will be well-positioned to make significant discoveries and contributions to the X-ray evolution and nature of the corona in transient accretion systems (as discussed in Section 6).

Finally, *HEX-P* will play a major role in the era of the high-resolution X-ray spectroscopy, with the development of microcalorimeters achieving a resolving power ($E/\Delta E$) larger than 1,000 at energies up to 7 keV. The Resolve instrument on *XRISM* (Tashiro et al., 2018; XRISM Science Team, 2022) launched in August 2023, and the X-ray Integral Field Unit (X-IFU) on *Athena*

(Nandra et al., 2013; Barret et al., 2023), expected to be launched in the late 2030s, will revolutionize our view of accretion onto compact objects. These instruments will probe the fine structure in absorption and emission from gas around accreting black holes. However, these gaseous structures are dictated by the hard ionizing X-rays, and the accurate measurements of such features will require a proper estimate of the underlying X-ray continuum out to tens of keV. This energy coverage can be provided by *NuSTAR* in the 2020s and *HEX-P* will extend and improve this coverage in the decades to come. In particular, *HEX-P* will be able to constrain the coronal emission and reflection spectrum at hard X-rays. This will be crucial for determining the illumination profile of the accretion disk by the X-ray corona, and accurately measuring BH spin for a broad range of mass and luminosity (see Piotrowska et al., 2023). Combining the resolving power of the future generation of microcalorimeters to the broad energy coverage of *HEX-P* will allow us to address important questions about black hole growth and evolution, and to understand the role of these objects in shaping the Universe.

9.2 Conclusion

We have demonstrated that *HEX-P* will provide an unprecedented look at the X-ray coronæ of accreting black holes with a main focus on AGN, thanks to its high sensitivity and broad energy coverage. The main results of the paper can be summarised as follows:

- *HEX-P* will accurately estimate the coronal properties of unobscured AGN. In particular, it will study evolution of coronal temperature in bright, variable AGN. This will allow us to measure the non-thermal fraction of electrons in AGN coronæ and test the runaway pair production hypothesis.
- *HEX-P* will also accurately estimate the coronal properties of obscured AGN up to $z \sim 0.5$. This will be a crucial test of the orientation-based unified model of AGN.
- *HEX-P* will efficiently constrain the coronal properties of high-redshift quasars ($z > 1.40$) even with high energy cutoff up to 200 keV. *HEX-P* will also extend the estimates of the coronal properties of powerful quasars beyond cosmic noon up to $z \simeq 4.5$. This will allow us to study the evolution of the X-ray properties of AGN across cosmic times.
- *HEX-P* will play a major role in studying transient events such as CLAGN and TDEs. It will allow us to witness the destruction, formation, and evolution of the X-ray corona in these extreme events.
- Finally, the high sensitivity of *HEX-P* that extends to hard X-rays and the possibility of long continuous observations of bright AGN will enable accurate reverberation mapping of the innermost regions of the accretion disk. This will allow us to estimate the location of the corona and its illuminating profile over a broad mass range.

Data availability statement

The raw data supporting the conclusion of this article will be made available by the authors, without undue reservation.

Author contributions

EK: Methodology, Visualization, Writing–original draft, Writing–review and editing. AL: Visualization, Writing–original draft, Writing–review and editing. MM: Writing–original draft, Writing–review and editing. DWi: Writing–original draft, Writing–review and editing. XZ: Writing–original draft, Writing–review and editing. MB: Writing–original draft, Writing–review and editing. PB: Writing–original draft, Writing–review and editing. RC: Writing–original draft, Writing–review and editing. PC: Conceptualization, Writing–review and editing. AF: Writing–review and editing. JG: Writing–original draft, Writing–review and editing. KM: Writing–original draft. NR: Investigation, Writing–review and editing. NS: Writing–original draft, Writing–review and editing. DS: Writing–review and editing. JT: Writing–review and editing. TW: Writing–review and editing. DWa: Writing–review and editing. SB: Writing–review and editing. JB: Writing–review and editing, Writing–original draft. FC: Writing–review and editing. GL: Writing–review and editing. LM: Writing–review and editing. GM: Writing–review and editing. AM: Writing–review and editing. EN: Writing–review and editing. JP: Writing–review and editing. CR: Writing–review and editing. K-WW: Writing–review and editing. AZ: Writing–review and editing.

Funding

Acknowledgments

Conflict of interest

The authors declare that the research was conducted in the absence of any commercial or financial relationships that could be construed as a potential conflict of interest.

The author(s) declared that they were an editorial board member of Frontiers, at the time of submission. This had no impact on the peer review process and the final decision.

The reviewer P-OP declared a past co-authorship with the authors SB, GM, and EK to the handling Editor.

Publisher's note

All claims expressed in this article are solely those of the authors and do not necessarily represent those of their affiliated organizations, or those of the publisher, the editors and the reviewers. Any product that may be evaluated in this article, or claim that may be made by its manufacturer, is not guaranteed or endorsed by the publisher.

References

Abazajian, K., Abdulghafour, A., Addison, G. E., Adshead, P., Ahmed, Z., Ajello, M., et al. (2022). *Snowmass 2021 CMB-S4 white paper*. arXiv e-prints, Available at: https://doi.org/10.48550/arXiv.2203.08024.

Agol, E., and Krolik, J. H. (2000). Magnetic stress at the marginally stable orbit: altered disk structure, radiation, and black hole spin evolution. *ApJ* 528, 161–170. doi:10.1086/308177

Ajello, M., Paliya, V., Marcotulli, L., Perkins, J. S., Prandini, E., D'Ammando, F., et al. (2019). Supermassive black holes at high redshifts. *BAAS* 51, 289.

Akylas, A., and Georgantopoulos, I. (2021). Distribution of the coronal temperature in Seyfert 1 galaxies. *A&A* 655, A60. doi:10.1051/0004-6361/202141186

Antonucci, R. (1993). Unified models for active galactic nuclei and quasars. *ARA&A* 31, 473–521. doi:10.1146/annurev.aa.31.090193.002353

Aversa, R., Lapi, A., de Zotti, G., Shankar, F., and Danese, L. (2015). Black hole and galaxy coevolution from continuity equation and abundance matching. *ApJ* 810, 74. doi:10.1088/0004-637X/810/1/74

Ballantyne, D. R., Bollenbacher, J. M., Brenneman, L. W., Madsen, K. K., Baloković, M., Boggs, S. E., et al. (2014). NuSTAR reveals the comptonizing corona of the broad-line radio galaxy 3C 382. *ApJ* 794, 62. doi:10.1088/0004-637X/794/1/62

Baloković, M., Brightman, M., Harrison, F. A., Comastri, A., Ricci, C., Buchner, J., et al. (2018). New spectral model for constraining torus covering factors from broadband X-ray spectra of active galactic nuclei. *ApJ* 854, 42. doi:10.3847/1538-4357/aaa7eb

Baloković, M., Harrison, F. A., Madejski, G., Comastri, A., Ricci, C., Annuar, A., et al. (2020). NuSTAR survey of obscured swift/BAT-selected active galactic nuclei. II. Median high-energy cutoff in Seyfert II hard X-ray spectra. *ApJ* 905, 41. doi:10.3847/1538-4357/abc342

Baloković, M., Matt, G., Harrison, F. A., Zoghbi, A., Ballantyne, D. R., Boggs, S. E., et al. (2015). Coronal properties of the Seyfert 1.9 galaxy MCG-05-23-016 determined from hard X-ray spectroscopy with NuSTAR. *ApJ* 800, 62. doi:10.1088/0004-637X/800/1/62

Barret, D., Albouys, V., Herder, J.-W. d., Piro, L., Cappi, M., Huovelin, J., et al. (2023). The Athena X-ray Integral Field Unit: a consolidated design for the system requirement review of the preliminary definition phase. *Exp. Astron.* 55, 373–426. doi:10.1007/s10686-022-09880-7

Barua, S., Jithesh, V., Misra, R., Dewangan, G. C., Sarma, R., and Pathak, A. (2020). NuSTAR observation of Ark 564 reveals the variation of coronal temperature with flux. *MNRAS* 492, 3041–3046. doi:10.1093/mnras/staa067

Baumgartner, W. H., Tueller, J., Markwardt, C. B., Skinner, G. K., Barthelmy, S., Mushotzky, R. F., et al. (2013). The 70 Month swift-BAT all-sky hard X-ray survey. *ApJS* 207, 19. doi:10.1088/0067-0049/207/2/19

Behar, E., Baldi, R. D., Laor, A., Horesh, A., Stevens, J., and Tzioumis, T. (2015). Discovery of millimetre-wave excess emission in radio-quiet active galactic nuclei. *MNRAS* 451, 517–526. doi:10.1093/mnras/stv988

Behar, E., Vogel, S., Baldi, R. D., Smith, K. L., and Mushotzky, R. F. (2018). The mm-wave compact component of an AGN. *MNRAS* 478, 399–406. doi:10.1093/mnras/sty850

Beheshtipour, B., Krawczynski, H., and Malzac, J. (2017). The X-ray polarization of the accretion disk coronae of active galactic nuclei. *ApJ* 850, 14. doi:10.3847/1538-4357/aa906a

Bellm, E. (2014). "The Zwicky transient facility," in *The third hot-wiring the transient universe workshop*. Editors P. R. Wozniak, M. J. Graham, A. A. Mahabal, and R. Seaman (Santa Fe: NASA/ADS), 27–33. doi:10.48550/arXiv.1410.8185

Belmont, R., Malzac, J., and Marcowith, A. (2008). Simulating radiation and kinetic processes in relativistic plasmas. *A&A* 491, 617–631. doi:10.1051/0004-6361:200809982

Beloborodov, A. M. (1999). Plasma ejection from magnetic flares and the X-ray spectrum of Cygnus X-1. *ApJ* 510, L123–L126. doi:10.1086/311810

Bentz, M. C., and Katz, S. (2015). The AGN black hole mass Database. *PASP* 127, 67–73. doi:10.1086/679601

Bertola, E., Vignali, C., Lanzuisi, G., Dadina, M., Cappi, M., Gilli, R., et al. (2022). The properties of the X-ray corona in the distant (z = 3.91) quasar APM 08279+5255. *A&A* 662, A98. doi:10.1051/0004-6361/202142642

Boorman, P. G., Torres-Albà, N., Annuar, A., Marchesi, S., Pfeifle, R., Stern, D., et al. (2023). The high energy X-ray probe (HEX-P): the circum-nuclear environment of growing supermassive black holes. *arXiv e-prints*, arXiv:2311.04949. doi:10.48550/arXiv.2311.04949

Brenneman, L. W., and Reynolds, C. S. (2006). Constraining black hole spin via X-ray spectroscopy. *ApJ* 652, 1028–1043. doi:10.1086/508146

Buchner, J., Brightman, M., Baloković, M., Wada, K., Bauer, F. E., and Nandra, K. (2021). Physically motivated X-ray obscurer models. *A&A* 651, A58. doi:10.1051/0004-6361/201834963

Buchner, J., Brightman, M., Nandra, K., Nikutta, R., and Bauer, F. E. (2019). X-ray spectral and eclipsing model of the clumpy obscurer in active galactic nuclei. *A&A* 629, A16. doi:10.1051/0004-6361/201834771

Buisson, D. J. K., Fabian, A. C., Barret, D., Fürst, F., Gandhi, P., García, J. A., et al. (2019). MAXI J1820+070 with NuSTAR I. An increase in variability frequency but a stable reflection spectrum: coronal properties and implications for the inner disc in black hole binaries. *MNRAS* 490, 1350–1362. doi:10.1093/mnras/stz2681

Buisson, D. J. K., Fabian, A. C., and Lohfink, A. M. (2018). Coronal temperatures of the AGN ESO 103-035 and IGR 2124.7+5058 from NuSTAR observations. *MNRAS* 481, 4419–4426. doi:10.1093/mnras/sty2609

Cackett, E. M., Zoghbi, A., Reynolds, C., Fabian, A. C., Kara, E., Uttley, P., et al. (2014). Modelling the broad Fe Kα reverberation in the AGN NGC 4151. *MNRAS* 438, 2980–2994. doi:10.1093/mnras/stt2424

Cadolle Bel, M., Sizun, P., Goldwurm, A., Rodriguez, J., Laurent, P., Zdziarski, A. A., et al. (2006). The broad-band spectrum of Cygnus X-1 measured by INTEGRAL. *A&A* 446, 591–602. doi:10.1051/0004-6361:20053068

Cangemi, F., Beuchert, T., Siegert, T., Rodriguez, J., Grinberg, V., Belmont, R., et al. (2021). Potential origin of the state-dependent high-energy tail in the black hole microquasar Cygnus X-1 as seen with INTEGRAL. *A&A* 650, A93. doi:10.1051/0004-6361/202038604

Carlstrom, J., Abazajian, K., Addison, G., Adshead, P., Ahmed, Z., Allen, S. W., et al. (2019). CMB-S4. *Bull. Am. Astronomical Soc.* 51, 209. doi:10.48550/arXiv.1908.01062

Chartas, G., Brandt, W. N., Gallagher, S. C., and Garmire, G. P. (2002). CHANDRA detects relativistic broad absorption lines from APM 08279+5255. *ApJ* 579, 169–175. doi:10.1086/342744

Chartas, G., Kochanek, C. S., Dai, X., Poindexter, S., and Garmire, G. (2009). X-ray microlensing in rxj1131-1231 and HE1104-1805. *ApJ* 693, 174–185. doi:10.1088/0004-637X/693/1/174

Chartas, G., Rhea, C., Kochanek, C., Dai, X., Morgan, C., Blackburne, J., et al. (2016). Gravitational lensing size scales for quasars. *Astron. Nachrichten* 337, 356–361. doi:10.1002/asna.201612313

Civano, F., Zhao, X., Boorman, P., Marchesi, S., Ananna, T., Creech, S., et al. (2023). The high energy X-ray probe (HEX-P): bringing the cosmic X-ray background into focus. arXiv e-prints. Available at: https://doi.org/10.48550/arXiv.2311.04832.

Connors, R., Tomsick, J., Draghis, P., Coughenour, B., Shaw, A., Garcia, J., et al. (2023). The high energy X-ray probe (HEX-P): probing accretion onto stellar mass black holes. arXiv e-prints, Available at: https://doi.org/10.48550/arXiv.2311.04782.

Coppi, P. S. (1999). "The physics of hybrid thermal/non-thermal plasmas," in *High energy processes in accreting black holes. Vol. 161 of astronomical society of the pacific conference series, 375*. Editors J. Poutanen, and R. Svensson (California, United States: Astronomical Society of the Pacific). doi:10.48550/arXiv.astro-ph/9903158

Dadina, M. (2007). BeppoSAX observations in the 2–100 keV band of the nearby Seyfert galaxies: an atlas of spectra. *A&A* 461, 1209–1252. doi:10.1051/0004-6361:20065734

Dauser, T., García, J., Parker, M. L., Fabian, A. C., Wilms, J., Lohfink, A., et al. (2020). *relxill: reflection models of black hole accretion disks*. record ascl:2010.015. Astrophysics Source Code Library.

Dauser, T., García, J., Walton, D. J., Eikmann, W., Kallman, T., McClintock, J., et al. (2016). Normalizing a relativistic model of X-ray reflection. Definition of the reflection fraction and its implementation in relxill. *A&A* 590, A76. doi:10.1051/0004-6361/201628135

Dauser, T., Garcia, J., Wilms, J., Böck, M., Brenneman, L. W., Falanga, M., et al. (2013). Irradiation of an accretion disc by a jet: general properties and implications for spin measurements of black holes. *MNRAS* 430, 1694–1708. doi:10.1093/mnras/sts710

De Marco, B., Ponti, G., Cappi, M., Dadina, M., Uttley, P., Cackett, E. M., et al. (2013). Discovery of a relation between black hole mass and soft X-ray time lags in active galactic nuclei. *MNRAS* 431, 2441–2452. doi:10.1093/mnras/stt339

de Rosa, A., Panessa, F., Bassani, L., Bazzano, A., Bird, A., Landi, R., et al. (2012). Broad-band study of hard X-ray-selected absorbed active galactic nuclei. *MNRAS* 420, 2087–2101. doi:10.1111/j.1365-2966.2011.20167.x

Di Matteo, T., Celotti, A., and Fabian, A. C. (1997). Cyclo-synchrotron emission from magnetically dominated active regions above accretion discs. *MNRAS* 291, 805–810. doi:10.1093/mnras/291.4.805

Doi, A., and Inoue, Y. (2016). High-frequency excess in the radio continuum spectrum of the type-1 Seyfert galaxy NGC 985. *PASJ* 68, 56. doi:10.1093/pasj/psw052

Done, C., Jin, C., Middleton, M., and Ward, M. (2013). A new way to measure supermassive black hole spin in accretion disc-dominated active galaxies. *MNRAS* 434, 1955–1963. doi:10.1093/mnras/stt1138

Dovčiak, M., Papadakis, I. E., Kammoun, E. S., and Zhang, W. (2022). Physical model for the broadband energy spectrum of X-ray illuminated accretion discs: fitting the spectral energy distribution of NGC 5548. *A&A* 661, A135. doi:10.1051/0004-6361/202142358

Elitzur, M., Ho, L. C., and Trump, J. R. (2014). Evolution of broad-line emission from active galactic nuclei. *MNRAS* 438, 3340–3351. doi:10.1093/mnras/stt2445

Emmanoulopoulos, D., Papadakis, I. E., Dovčiak, M., and McHardy, I. M. (2014). General relativistic modelling of the negative reverberation X-ray time delays in AGN. *MNRAS* 439, 3931–3950. doi:10.1093/mnras/stu249

Eraerds, T., Antonelli, V., Davis, C., Hall, D., Hetherington, O., Holland, A., et al. (2021). Enhanced simulations on the athena/wide field imager instrumental background. *J. Astronomical Telesc. Instrum. Syst.* 7, 034001. doi:10.1117/1.JATIS.7.3.034001

Fabian, A. C., and Iwasawa, K. (1999). The mass density in black holes inferred from the X-ray background. *MNRAS* 303, L34–L36. doi:10.1046/j.1365-8711.1999.02404.x

Fabian, A. C., Lohfink, A., Belmont, R., Malzac, J., and Coppi, P. (2017). Properties of AGN coronae in the NuSTAR era - II. Hybrid plasma. *MNRAS* 467, 2566–2570. doi:10.1093/mnras/stx221

Fabian, A. C., Lohfink, A., Kara, E., Parker, M. L., Vasudevan, R., and Reynolds, C. S. (2015). Properties of AGN coronae in the NuSTAR era. *MNRAS* 451, 4375–4383. doi:10.1093/mnras/stv1218

Fabian, A. C., Parker, M. L., Wilkins, D. R., Miller, J. M., Kara, E., Reynolds, C. S., et al. (2014). On the determination of the spin and disc truncation of accreting black holes using X-ray reflection. *MNRAS* 439, 2307–2313. doi:10.1093/mnras/stu045

Fabian, A. C., Rees, M. J., Stella, L., and White, N. E. (1989). X-ray fluorescence from the inner disc in Cygnus X-1. *MNRAS* 238, 729–736. doi:10.1093/mnras/238.3.729

Fabian, A. C., Zoghbi, A., Ross, R. R., Uttley, P., Gallo, L. C., Brandt, W. N., et al. (2009). Broad line emission from iron K- and L-shell transitions in the active galaxy 1H0707-495. *Nature* 459, 540–542. doi:10.1038/nature08007

Fabian, A. C., Zoghbi, A., Wilkins, D., Dwelly, T., Uttley, P., Schartel, N., et al. (2012). 1H 0707-495 in 2011: an X-ray source within a gravitational radius of the event horizon. *MNRAS* 419, 116–123. doi:10.1111/j.1365-2966.2011.19676.x

Falcke, H., Körding, E., and Markoff, S. (2004). A scheme to unify low-power accreting black holes. Jet-dominated accretion flows and the radio/X-ray correlation. *A&A* 414, 895–903. doi:10.1051/0004-6361:20031683

Galeev, A. A., Rosner, R., and Vaiana, G. S. (1979). Structured coronae of accretion disks. *ApJ* 229, 318–326. doi:10.1086/156957

Gallo, L. (2018). X-ray perspective of Narrow-line Seyfert 1 galaxies. *Revisiting Narrow-Line Seyfert 1 Galaxies their Place Universe* 328, 35. doi:10.22323/1.328.0034

Gallo, L. C. (2006). Investigating the nature of narrow-line Seyfert 1 galaxies with high-energy spectral complexity. *MNRAS* 368, 479–486. doi:10.1111/j.1365-2966.2006.10137.x

Gallo, L. C., Gonzalez, A. G., and Miller, J. M. (2021). Eclipsing the X-ray emitting region in the active galaxy NGC 6814. *ApJ* 908, L33. doi:10.3847/2041-8213/abdcb5

García, J., Dauser, T., Lohfink, A., Kallman, T. R., Steiner, J. F., McClintock, J. E., et al. (2014). Improved reflection models of black hole accretion disks: treating the angular distribution of X-rays. *ApJ* 782, 76. doi:10.1088/0004-637X/782/2/76

García, J., Dauser, T., Reynolds, C. S., Kallman, T. R., McClintock, J. E., Wilms, J., et al. (2013). X-ray reflected spectra from accretion disk models. III. A complete grid of ionized reflection calculations. *ApJ* 768, 146. doi:10.1088/0004-637X/768/2/146

García, J. A., Dauser, T., Steiner, J. F., McClintock, J. E., Keck, M. L., and Wilms, J. (2015). On estimating the high-energy cutoff in the x-ray spectra of black holes via reflection spectroscopy. *Astrophysical J. Lett.* 808, L37. doi:10.1088/2041-8205/808/2/L37

Ghisellini, G., Haardt, F., and Fabian, A. C. (1993). On re-acceleration, pairs and the high-energy spectrum of AGN and galactic black hole candidates. *MNRAS* 263, L9–L12. doi:10.1093/mnras/263.1.L9

Ghisellini, G., Haardt, F., and Matt, G. (1994). The contribution of the obscuring torus to the X-ray spectrum of Seyfert galaxies: a test for the unification model. *MNRAS* 267, 743–754. doi:10.1093/mnras/267.3.743

Ghisellini, G., Haardt, F., and Matt, G. (2004). Aborted jets and the X-ray emission of radio-quiet AGNs. *A&A* 413, 535–545. doi:10.1051/0004-6361:20031562

Gianolli, V. E., Kim, D. E., Bianchi, S., Agís-González, B., Madejski, G., Marin, F., et al. (2023). Uncovering the geometry of the hot X-ray corona in the Seyfert galaxy NGC 4151 with IXPE. *MNRAS* 523, 4468–4476. doi:10.1093/mnras/stad1697

Gilli, R., Comastri, A., and Hasinger, G. (2007). The synthesis of the cosmic X-ray background in the Chandra and XMM-Newton era. *A&A* 463, 79–96. doi:10.1051/0004-6361:20066334

Gonzalez, A. G., Wilkins, D. R., and Gallo, L. C. (2017). Probing the geometry and motion of AGN coronae through accretion disc emissivity profiles. *MNRAS* 472, 1932–1945. doi:10.1093/mnras/stx2080

Goosmann, R. W., and Matt, G. (2011). Spotting the misaligned outflows in NGC 1068 using X-ray polarimetry. *MNRAS* 415, 3119–3128. doi:10.1111/j.1365-2966.2011.18923.x

Graham, M. J., Kulkarni, S. R., Bellm, E. C., Adams, S. M., Barbarino, C., Blagorodnova, N., et al. (2019). The Zwicky transient facility: science objectives. *PASP* 131, 078001. doi:10.1088/1538-3873/ab006c

Guedel, M., and Benz, A. O. (1993). X-Ray/Microwave relation of different types of active stars. *ApJ* 405, L63. doi:10.1086/186766

Guilbert, P. W., Fabian, A. C., and Rees, M. J. (1983). Spectral and variability constraints on compact sources. *MNRAS* 205, 593–603. doi:10.1093/mnras/205.3.593

Gupta, S., Sridhar, N., and Sironi, L. (2023). Comptonization by reconnection plasmoids in black hole coronae III: dependence on the guide field in pair plasma. arXiv e-prints, Available at: https://doi.org/10.48550/arXiv.2310.04233.

Haardt, F., and Maraschi, L. (1991). A two-phase model for the X-ray emission from Seyfert galaxies. *ApJ* 380, L51. doi:10.1086/186171

Haardt, F., and Maraschi, L. (1993). X-ray spectra from two-phase accretion disks. *ApJ* 413, 507. doi:10.1086/173020

Harrison, F. A., Craig, W. W., Christensen, F. E., Hailey, C. J., Zhang, W. W., Boggs, S. E., et al. (2013). The nuclear spectroscopic telescope Array (NuSTAR) high-energy X-ray mission. *ApJ* 770, 103. doi:10.1088/0004-637X/770/2/103

Henri, G., and Pelletier, G. (1991). Relativistic electron-positron beam formation in the framework of the two-flow model for active galactic nuclei. *ApJ* 383, L7. doi:10.1086/186228

Henri, G., and Petrucci, P. O. (1997). Anisotropic illumination of AGN's accretion disk by a non thermal source. I. General theory and application to the Newtonian geometry. *A&A* 326, 87–98. doi:10.48550/arXiv.astro-ph/9705233

Hickox, R. C., and Alexander, D. M. (2018). Obscured active galactic nuclei. *ARA&A* 56, 625–671. doi:10.1146/annurev-astro-081817-051803

Ingram, A., Ewing, M., Marinucci, A., Tagliacozzo, D., Rosario, D. J., Veledina, A., et al. (2023). The X-ray polarisation of the Seyfert 1 galaxy IC 4329A. arXiv e-prints, Available at: https://doi.org/10.48550/arXiv.2305.13028.

Ingram, A., Mastroserio, G., Dauser, T., Hovenkamp, P., van der Klis, M., and García, J. A. (2019). A public relativistic transfer function model for X-ray reverberation mapping of accreting black holes. *MNRAS* 488, 324–347. doi:10.1093/mnras/stz1720

Inoue, Y., and Doi, A. (2014). Unveiling the nature of coronae in active galactic nuclei through submillimeter observations. *PASJ* 66, L8. doi:10.1093/pasj/psu079

Inoue, Y., and Doi, A. (2018). Detection of coronal magnetic activity in nearby active supermassive black holes. *ApJ* 869, 114. doi:10.3847/1538-4357/aaeb95

Jahoda, K., Krawczynski, H., Kislat, F., Marshall, H., Okajima, T., Agudo, I., et al. (2019). The X-ray Polarization Probe mission concept. arXiv e-prints , Available at: https://doi.org/10.48550/arXiv.1907.10190.

Jansen, F., Lumb, D., Altieri, B., Clavel, J., Ehle, M., Erd, C., et al. (2001). XMM-Newton observatory. I. The spacecraft and operations. *A&A* 365, L1–L6. doi:10.1051/0004-6361:20000036

Jiang, J., Parker, M. L., Fabian, A. C., Alston, W. N., Buisson, D. J. K., Cackett, E. M., et al. (2018). The 1.5 Ms observing campaign on IRAS 13224-3809 - I. X-ray spectral analysis. *MNRAS* 477, 3711–3726. doi:10.1093/mnras/sty836

Kammoun, E. S., Igo, Z., Miller, J. M., Fabian, A. C., Reynolds, M. T., Merloni, A., et al. (2023). The first X-ray look at SMSS J114447.77-430859.3: the most luminous quasar in the last 9 Gyr. *MNRAS* 522, 5217–5237. doi:10.1093/mnras/stad952

Kammoun, E. S., Miller, J. M., Koss, M., Oh, K., Zoghbi, A., Mushotzky, R. F., et al. (2020). A hard look at local, optically selected, obscured Seyfert galaxies. *ApJ* 901, 161. doi:10.3847/1538-4357/abb29f

Kammoun, E. S., Risaliti, G., Stern, D., Jun, H. D., Graham, M., Celotti, A., et al. (2017). Coronal properties of the luminous radio-quiet quasar QSO B2202-209. *MNRAS* 465, 1665–1671. doi:10.1093/mnras/stw2897

Kamraj, N., Brightman, M., Harrison, F. A., Stern, D., García, J. A., Baloković, M., et al. (2022). X-ray coronal properties of swift/BAT-selected Seyfert 1 active galactic nuclei. *ApJ* 927, 42. doi:10.3847/1538-4357/ac45f6

Kamraj, N., Harrison, F. A., Baloković, M., Lohfink, A., and Brightman, M. (2018). Coronal properties of swift/BAT-selected Seyfert 1 AGNs observed with NuSTAR. *ApJ* 866, 124. doi:10.3847/1538-4357/aad0d0

Kara, E., Alston, W. N., Fabian, A. C., Cackett, E. M., Uttley, P., Reynolds, C. S., et al. (2016). A global look at X-ray time lags in Seyfert galaxies. *MNRAS* 462, 511–531. doi:10.1093/mnras/stw1695

Kara, E., García, J. A., Lohfink, A., Fabian, A. C., Reynolds, C. S., Tombesi, F., et al. (2017). The high-Eddington NLS1 Ark 564 has the coolest corona. *MNRAS* 468, 3489–3498. doi:10.1093/mnras/stx792

Kara, E., Zoghbi, A., Marinucci, A., Walton, D. J., Fabian, A. C., Risaliti, G., et al. (2015). Iron K and Compton hump reverberation in SWIFT J2127.4+5654 and NGC 1365 revealed by NuSTAR and XMM-Newton. *MNRAS* 446, 737–749. doi:10.1093/mnras/stu2136

Kawamuro, T., Ricci, C., Imanishi, M., Mushotzky, R. F., Izumi, T., Ricci, F., et al. (2022). BASS XXXII: studying the nuclear millimeter-wave continuum emission of AGNs with ALMA at scales ≲100-200 pc. *ApJ* 938, 87. doi:10.3847/1538-4357/ac8794

Kawamuro, T., Ricci, C., Mushotzky, R. F., Imanishi, M., Bauer, F. E., Ricci, F., et al. (2023). BASS XXXIV: a catalog of the nuclear mm-wave continuum emission properties of AGNs constrained on scales ≲ 100–200 pc. arXiv e-prints, Available at: https://doi.org/10.48550/arXiv.2309.02776.

Kochanek, C. S., Dai, X., Morgan, C., Morgan, N., Poindexter, G., and Chartas, S. (2007). "Turning AGN microlensing from a curiosity into a tool," in *Statistical challenges in modern astronomy IV*. Editors G. J Babu, and E. D Feigelson. vol. 371 of Astronomical Society of the Pacific Conference Series, 43. doi:10.48550/arXiv.astro-ph/0609112

Körding, E. G., Jester, S., and Fender, R. (2006). Accretion states and radio loudness in active galactic nuclei: analogies with X-ray binaries. *MNRAS* 372, 1366–1378. doi:10.1111/j.1365-2966.2006.10954.x

Koss, M. J., Ricci, C., Trakhtenbrot, B., Oh, K., den Brok, J. S., Mejía-Restrepo, J. E., et al. (2022). BASS. XXII. The BASS DR2 AGN catalog and data. *ApJS* 261, 2. doi:10.3847/1538-4365/ac6c05

Krawczynski, H., Matt, G., Ingram, A. R., Taverna, R., Turolla, R., Kislat, F., et al. (2019). Astro2020 science white paper: using X-ray polarimetry to probe the physics of black holes and neutron stars. arXiv e-prints, Available at: https://doi.org/10.48550/arXiv.1904.09313.

Krawczynski, H., Muleri, F., Dovčiak, M., Veledina, A., Rodriguez Cavero, N., Svoboda, J., et al. (2022). Polarized x-rays constrain the disk-jet geometry in the black hole x-ray binary Cygnus X-1. *Science* 378, 650–654. doi:10.1126/science.add5399

Laha, S., Meyer, E., Roychowdhury, A., Becerra Gonzalez, J., Acosta-Pulido, J. A., Thapa, A., et al. (2022). A radio, optical, UV, and X-ray view of the enigmatic changing-look active galactic nucleus 1ES 1927+654 from its pre-to postflare states. *ApJ* 931, 5. doi:10.3847/1538-4357/ac63aa

Lanzuisi, G., Gilli, R., Cappi, M., Dadina, M., Bianchi, S., Brusa, M., et al. (2019). NuSTAR measurement of coronal temperature in two luminous, high-redshift quasars. *ApJ* 875, L20. doi:10.3847/2041-8213/ab15dc

Laor, A., and Behar, E. (2008). On the origin of radio emission in radio-quiet quasars. *MNRAS* 390, 847–862. doi:10.1111/j.1365-2966.2008.13806.x

Lewin, C., Kara, E., Wilkins, D., Mastroserio, G., García, J. A., Zhang, R. C., et al. (2022). X-ray reverberation mapping of Ark 564 using Gaussian process regression. *ApJ* 939, 109. doi:10.3847/1538-4357/ac978f

Liu, T., Wang, J.-X., Yang, H., Zhu, F.-F., and Zhou, Y.-Y. (2014). Are X-ray emitting coronae around supermassive black holes outflowing? *ApJ* 783, 106. doi:10.1088/0004-637X/783/2/106

Liu, Z., Malyali, A., Krumpe, M., Homan, D., Goodwin, A. J., Grotova, I., et al. (2023). Deciphering the extreme X-ray variability of the nuclear transient eRASSt J045650.3−203750. A likely repeating partial tidal disruption event. *A&A* 669, A75. doi:10.1051/0004-6361/202244805

Lubiński, P., Beckmann, V., Gibaud, L., Paltani, S., Papadakis, I. E., Ricci, C., et al. (2016). A comprehensive analysis of the hard X-ray spectra of bright Seyfert galaxies. *MNRAS* 458, 2454–2475. doi:10.1093/mnras/stw454

Lusso, E., Comastri, A., Simmons, B. D., Mignoli, M., Zamorani, G., Vignali, C., et al. (2012). Bolometric luminosities and Eddington ratios of X-ray selected active galactic nuclei in the XMM-COSMOS survey. *MNRAS* 425, 623–640. doi:10.1111/j.1365-2966.2012.21513.x

Lusso, E., and Risaliti, G. (2016). The tight relation between X-ray and ultraviolet luminosity of quasars. *ApJ* 819, 154. doi:10.3847/0004-637X/819/2/154

Madsen, K. K., García, J. A., Stern, D., Armini, R., Basso, S., Coutinho, D., et al. (2023). The high energy X-ray probe (HEX-P): instrument and mission profile. *arXiv e-prints*, arXiv:2312.04678. doi:10.48550/arXiv.2312.04678

Malizia, A., Molina, M., Bassani, L., Stephen, J. B., Bazzano, A., Ubertini, P., et al. (2014). The INTEGRAL high-energy cut-off distribution of type 1 active galactic nuclei. *ApJ* 782, L25. doi:10.1088/2041-8205/782/2/L25

Mallick, L., Alston, W. N., Parker, M. L., Fabian, A. C., Pinto, C., Dewangan, G. C., et al. (2018). A high-density relativistic reflection origin for the soft and hard X-ray excess emission from Mrk 1044. *MNRAS* 479, 615–634. doi:10.1093/mnras/sty1487

Mallick, L., Fabian, A. C., García, J. A., Tomsick, J. A., Parker, M. L., Dauser, T., et al. (2022). High-density disc reflection spectroscopy of low-mass active galactic nuclei. *MNRAS* 513, 4361–4379. doi:10.1093/mnras/stac990

Mallick, L., Wilkins, D. R., Alston, W. N., Markowitz, A., De Marco, B., Parker, M. L., et al. (2021). Discovery of soft and hard X-ray time lags in low-mass AGNs. *MNRAS* 503, 3775–3783. doi:10.1093/mnras/stab627

Malzac, J., Beloborodov, A. M., and Poutanen, J. (2001). X-ray spectra of accretion discs with dynamic coronae. *MNRAS* 326, 417–427. doi:10.1046/j.1365-8711.2001.04450.x

Marconi, A., Risaliti, G., Gilli, R., Hunt, L. K., Maiolino, R., and Salvati, M. (2004). Local supermassive black holes, relics of active galactic nuclei and the X-ray background. *MNRAS* 351, 169–185. doi:10.1111/j.1365-2966.2004.07765.x

Marcotulli, L., Ajello, M., Böttcher, M., Coppi, P., Costamante, L., Di Gesu, L., et al. (2023). The High Energy X-ray Probe (HEX-P): the most powerful jets through the lens of a superb X-ray eye. arXiv e-prints, Available at: https://doi.org/10.48550/arXiv.2311.04801.

Marin, F., Dovčiak, M., Muleri, F., Kislat, F. F., and Krawczynski, H. S. (2018). Predicting the X-ray polarization of type 2 Seyfert galaxies. *MNRAS* 473, 1286–1316. doi:10.1093/mnras/stx2382

Marinucci, A., Muleri, F., Dovciak, M., Bianchi, S., Marin, F., Matt, G., et al. (2022a). Polarization constraints on the X-ray corona in Seyfert galaxies: MCG-05-23-16. *MNRAS* 516, 5907–5913. doi:10.1093/mnras/stac2634

Marinucci, A., Vietri, G., Piconcelli, E., Bianchi, S., Guainazzi, M., Lanzuisi, G., et al. (2022b). Breaking the rules at z ≃ 0.45: the rebel case of RBS 1055. *A&A* 666, A169. doi:10.1051/0004-6361/202244272

Markoff, S., Nowak, M. A., and Wilms, J. (2005). Going with the flow: can the base of jets subsume the role of compact accretion disk coronae? *ApJ* 635, 1203–1216. doi:10.1086/497628

Martocchia, A., and Matt, G. (1996). Iron Kα line intensity from accretion discs around rotating black holes. *MNRAS* 282, L53–L57. doi:10.1093/mnras/282.4.L53

Masterson, M., Kara, E., Ricci, C., García, J. A., Fabian, A. C., Pinto, C., et al. (2022). Evolution of a relativistic outflow and X-ray corona in the extreme changing-look AGN 1ES 1927+654. *ApJ* 934, 35. doi:10.3847/1538-4357/ac76c0

Mastroserio, G., Ingram, A., and van der Klis, M. (2020). Multi-timescale reverberation mapping of Mrk 335. *MNRAS* 498, 4971–4982. doi:10.1093/mnras/staa2735

Mastroserio, G., Ingram, A., Wang, J., García, J. A., van der Klis, M., Cavecchi, Y., et al. (2021). Modelling correlated variability in accreting black holes: the effect of high density and variable ionization on reverberation lags. *MNRAS* 507, 55–73. doi:10.1093/mnras/stab2056

Matt, G., Marinucci, A., Guainazzi, M., Brenneman, L. W., Elvis, M., Lohfink, A., et al. (2014). The soft-X-ray emission of Ark 120. XMM-Newton, NuSTAR, and the importance of taking the broad view. *MNRAS* 439, 3016–3021. doi:10.1093/mnras/stu159

Matt, G., Perola, G. C., and Piro, L. (1991). The iron line and high energy bump as X-ray signatures of cold matter in Seyfert 1 galaxies. *A&A* 247, 25.

McHardy, I. M., Koerding, E., Knigge, C., Uttley, P., and Fender, R. P. (2006). Active galactic nuclei as scaled-up Galactic black holes. *Nature* 444, 730–732. doi:10.1038/nature05389

Meidinger, N., Albrecht, S., Beitler, C., Bonholzer, M., Emberger, V., Frank, J., et al. (2020). "Development status of the wide field imager instrument for Athena," in *Society of photo-optical instrumentation engineers (SPIE) conference series*. vol. 11444 of Society of Photo-Optical Instrumentation Engineers (SPIE) Conference Series. doi:10.1117/12.2560507

Merloni, A., Dwelly, T., Salvato, M., Georgakakis, A., Greiner, J., Krumpe, M., et al. (2015). A tidal disruption flare in a massive galaxy? Implications for the fuelling mechanisms of nuclear black holes. *MNRAS* 452, 69–87. doi:10.1093/mnras/stv1095

Merloni, A., and Fabian, A. C. (2001a). Accretion disc coronae as magnetic reservoirs. *MNRAS* 321, 549–552. doi:10.1046/j.1365-8711.2001.04060.x

Merloni, A., and Fabian, A. C. (2001b). Thunderclouds and accretion discs: a model for the spectral and temporal variability of Seyfert 1 galaxies. *MNRAS* 328, 958–968. doi:10.1046/j.1365-8711.2001.04925.x

Middei, R., Bianchi, S., Marinucci, A., Matt, G., Petrucci, P. O., Tamborra, F., et al. (2019). Relations between phenomenological and physical parameters in the hot coronae of AGNs computed with the MoCA code. *A&A* 630, A131. doi:10.1051/0004-6361/201935881

Miniutti, G., and Fabian, A. C. (2004). A light bending model for the X-ray temporal and spectral properties of accreting black holes. *MNRAS* 349, 1435–1448. doi:10.1111/j.1365-2966.2004.07611.x

Molina, M., Bassani, L., Malizia, A., Stephen, J. B., Bird, A. J., Bazzano, A., et al. (2013). Hard-X-ray spectra of active galactic nuclei in the INTEGRAL complete sample. *MNRAS* 433, 1687–1700. doi:10.1093/mnras/stt844

Mosquera, A. M., Kochanek, C. S., Chen, B., Dai, X., Blackburne, J. A., and Chartas, G. (2013). The structure of the X-ray and optical emitting regions of the lensed quasar Q 2237+0305. *ApJ* 769, 53. doi:10.1088/0004-637X/769/1/53

Nandra, K., Barret, D., Barcons, X., Fabian, A., den Herder, J.-W., Piro, L., et al. (2013). The hot and energetic universe: a white paper presenting the science theme motivating the Athena+ mission. arXiv e-prints, Available at: https://doi.org/10.48550/arXiv.1306.2307.

Nicastro, F., Piro, L., De Rosa, A., Feroci, M., Grandi, P., Fiore, F., et al. (2000). A long observation of NGC 5548 by BeppoSAX: the high-energy cutoff, intrinsic spectral variability, and a truly warm absorber. *ApJ* 536, 718–728. doi:10.1086/308950

Niedźwiecki, A., Zdziarski, A. A., and Szanecki, M. (2016). On the lamppost model of accreting black holes. *ApJ* 821, L1. doi:10.3847/2041-8205/821/1/L1

Noda, H., and Done, C. (2018). Explaining changing-look AGN with state transition triggered by rapid mass accretion rate drop. *MNRAS* 480, 3898–3906. doi:10.1093/mnras/sty2032

Oh, K., Koss, M., Markwardt, C. B., Schawinski, K., Baumgartner, W. H., Barthelmy, S. D., et al. (2018). The 105-month swift-BAT all-sky hard X-ray survey. *ApJS* 235, 4. doi:10.3847/1538-4365/aaa7fd

Panessa, F., Baldi, R. D., Laor, A., Padovani, P., Behar, E., and McHardy, I. (2019). The origin of radio emission from radio-quiet active galactic nuclei. *Nat. Astron.* 3, 387–396. doi:10.1038/s41550-019-0765-4

Parker, M. L., Wilkins, D. R., Fabian, A. C., Grupe, D., Dauser, T., Matt, G., et al. (2014). The NuSTAR spectrum of Mrk 335: extreme relativistic effects within two gravitational radii of the event horizon? *MNRAS* 443, 1723–1732. doi:10.1093/mnras/stu1246

Pasham, D. R., Remillard, R. A., Fragile, P. C., Franchini, A., Stone, N. C., Lodato, G., et al. (2019). A loud quasi-periodic oscillation after a star is disrupted by a massive black hole. *Science* 363, 531–534. doi:10.1126/science.aar7480

Petrucci, P. O., Gronkiewicz, D., Rozanska, A., Belmont, R., Bianchi, S., Czerny, B., et al. (2020). Radiation spectra of warm and optically thick coronae in AGNs. *A&A* 634, A85. doi:10.1051/0004-6361/201937011

Petrucci, P. O., Haardt, F., Maraschi, L., Grandi, P., Malzac, J., Matt, G., et al. (2001a). Testing comptonization models using BeppoSAX observations of Seyfert 1 galaxies. *ApJ* 556, 716–726. doi:10.1086/321629

Petrucci, P. O., Maraschi, L., Haardt, F., and Nandra, K. (2004). Physical interpretation of the NGC 7469 UV/X-ray variability. *A&A* 413, 477–487. doi:10.1051/0004-6361:20031499

Petrucci, P. O., Merloni, A., Fabian, A., Haardt, F., and Gallo, E. (2001b). The effects of a Comptonizing corona on the appearance of the reflection components in accreting black hole spectra. *MNRAS* 328, 501–510. doi:10.1046/j.1365-8711.2001.04897.x

Petrucci, P. O., Paltani, S., Malzac, J., Kaastra, J. S., Cappi, M., Ponti, G., et al. (2013). Multiwavelength campaign on Mrk 509. XII. Broad band spectral analysis. *A&A* 549, A73. doi:10.1051/0004-6361/201219956

Petrucci, P. O., Piétu, V., Behar, E., Clavel, M., Bianchi, S., Henri, G., et al. (2023). Simultaneous millimetric and X-ray intraday variability in the radio-quiet AGN MCG+08-11-11. *A&A* 678, L4. doi:10.1051/0004-6361/202347495

Petrucci, P. O., Ursini, F., De Rosa, A., Bianchi, S., Cappi, M., Matt, G., et al. (2018). Testing warm Comptonization models for the origin of the soft X-ray excess in AGNs. *A&A* 611, A59. doi:10.1051/0004-6361/201731580

Piotrowska, J. M., García, J. A., Walton, D. J., Beckmann, R. S., Stern, D., Ballantyne, D. R., et al. (2023). The high energy X-ray probe (HEX-P): constraining supermassive black hole growth with population spin measurements. arXiv e-prints, Available at: https://doi.org/10.48550/arXiv.2311.04752.

Porquet, D., Done, C., Reeves, J. N., Grosso, N., Marinucci, A., Matt, G., et al. (2019). A deep X-ray view of the bare AGN Ark 120. V. Spin determination from disc-Comptonisation efficiency method. *A&A* 623, A11. doi:10.1051/0004-6361/201834448

Poutanen, J., and Svensson, R. (1996). The two-phase pair corona model for active galactic nuclei and X-ray binaries: how to obtain exact solutions. *ApJ* 470, 249. doi:10.1086/177865

Predehl, P., Andritschke, R., Arefiev, V., Babyshkin, V., Batanov, O., Becker, W., et al. (2021). The eROSITA X-ray telescope on SRG. *A&A* 647, A1. doi:10.1051/0004-6361/202039313

Raginski, I., and Laor, A. (2016). AGN coronal emission models - I. The predicted radio emission. *MNRAS* 459, 2082–2096. doi:10.1093/mnras/stw772

Raimundo, S. I., and Fabian, A. C. (2009). Eddington ratio and accretion efficiency in active galactic nuclei evolution. *MNRAS* 396, 1217–1221. doi:10.1111/j.1365-2966.2009.14796.x

Raimundo, S. I., Fabian, A. C., Vasudevan, R. V., Gandhi, P., and Wu, J. (2012). Can we measure the accretion efficiency of active galactic nuclei? *MNRAS* 419, 2529–2544. doi:10.1111/j.1365-2966.2011.19904.x

Ratheesh, A., Matt, G., Tombesi, F., Soffitta, P., Pesce-Rollins, M., and Di Marco, A. (2021). Exploring the accretion-ejection geometry of GRS 1915+105 in the obscured state with future X-ray spectro-polarimetry. *A&A* 655, A96. doi:10.1051/0004-6361/202140701

Reeves, J. N., Braito, V., Porquet, D., Lobban, A. P., Matzeu, G. A., and Nardini, E. (2021). The flaring X-ray corona in the quasar PDS 456. *MNRAS* 500, 1974–1991. –1991. doi:10.1093/mnras/staa3377

Reis, R. C., and Miller, J. M. (2013). On the size and location of the X-ray emitting coronae around black holes. *ApJ* 769, L7. doi:10.1088/2041-8205/769/1/L7

Remillard, R. A., and McClintock, J. E. (2006). X-ray properties of black-hole binaries. *ARA&A* 44, 49–92. doi:10.1146/annurev.astro.44.051905.092532

Reynolds, C. S. (2021). Observational constraints on black hole spin. *ARA&A* 59, 117–154. doi:10.1146/annurev-astro-112420-035022

Reynolds, C. S., and Begelman, M. C. (1997). Iron fluorescence from within the innermost stable orbit of black hole accretion disks. *ApJ* 488, 109–118. doi:10.1086/304703

Ricci, C., Chang, C.-S., Kawamuro, T., Privon, G., Mushotzky, R., Trakhtenbrot, B., et al. (2023). A tight correlation between millimeter and X-ray emission in accreting massive black holes from < 100 milliarcsecond-resolution ALMA observations. arXiv e-prints , Available at: https://doi.org/10.48550/arXiv.2306.04679.

Ricci, C., Ho, L. C., Fabian, A. C., Trakhtenbrot, B., Koss, M. J., Ueda, Y., et al. (2018). BAT AGN Spectroscopic Survey - XII. The relation between coronal properties of active galactic nuclei and the Eddington ratio. *MNRAS* 480, 1819–1830. doi:10.1093/mnras/sty1879

Ricci, C., Kara, E., Loewenstein, M., Trakhtenbrot, B., Arcavi, I., Remillard, R., et al. (2020). The destruction and recreation of the X-ray corona in a changing-look active galactic nucleus. *ApJ* 898, L1. doi:10.3847/2041-8213/ab91a1

Ricci, C., Loewenstein, M., Kara, E., Remillard, R., Trakhtenbrot, B., Arcavi, I., et al. (2021). The 450 Day X-ray monitoring of the changing-look AGN 1ES 1927+654. *ApJS* 255, 7. doi:10.3847/1538-4365/abe94b

Ricci, C., and Trakhtenbrot, B. (2022). Changing-look active galactic nuclei. arXiv e-prints, Available at: https://doi.org/10.48550/arXiv.2211.05132.

Ricci, C., Trakhtenbrot, B., Koss, M. J., Ueda, Y., Del Vecchio, I., Treister, E., et al. (2017). BAT AGN spectroscopic survey. V. X-ray properties of the Swift/BAT 70-month AGN catalog. *ApJS* 233, 17. doi:10.3847/1538-4365/aa96ad

Risaliti, G., Harrison, F. A., Madsen, K. K., Walton, D. J., Boggs, S. E., Christensen, F. E., et al. (2013). A rapidly spinning supermassive black hole at the centre of NGC 1365. *Nature* 494, 449–451. doi:10.1038/nature11938

Risaliti, G., Nardini, E., Salvati, M., Elvis, M., Fabbiano, G., Maiolino, R., et al. (2011). X-ray absorption by broad-line region clouds in Mrk 766. *MNRAS* 410, 1027–1035. doi:10.1111/j.1365-2966.2010.17503.x

Rivers, E., Markowitz, A., and Rothschild, R. (2013). Full spectral survey of active galactic nuclei in the rossi X-ray timing explorer archive. *ApJ* 772, 114. doi:10.1088/0004-637X/772/2/114

Ross, N. P., Ford, K. E. S., Graham, M., McKernan, B., Stern, D., Meisner, A. M., et al. (2018). A new physical interpretation of optical and infrared variability in quasars. *MNRAS* 480, 4468–4479. doi:10.1093/mnras/sty2002

Ruan, J. J., Anderson, S. F., Eracleous, M., Green, P. J., Haggard, D., MacLeod, C. L., et al. (2019). The analogous structure of accretion flows in supermassive and stellar mass black holes: new insights from faded changing-look quasars. *ApJ* 883, 76. doi:10.3847/1538-4357/ab3c1a

Rybicki, G. B., and Lightman, A. P. (1979). *Radiative processes in astrophysics*. New Jersey: John Wiley and Sons, Ltd.

Sagiv, I., Gal-Yam, A., Ofek, E. O., Waxman, E., Aharonson, O., Kulkarni, S. R., et al. (2014). Science with a wide-field UV transient explorer. *AJ* 147, 79. doi:10.1088/0004-6256/147/4/79

Sanfrutos, M., Miniutti, G., Agís-González, B., Fabian, A. C., Miller, J. M., Panessa, F., et al. (2013). The size of the X-ray emitting region in SWIFT J2127.4+5654 via a broad line region cloud X-ray eclipse. *MNRAS* 436, 1588–1594. doi:10.1093/mnras/stt1675

Saxton, R. D., Read, A. M., Esquej, P., Komossa, S., Dougherty, S., Rodriguez-Pascual, P., et al. (2012). A tidal disruption-like X-ray flare from the quiescent galaxy SDSS J120136.02+300305.5⋆. *Astronomy Astrophysics* 541, A106. doi:10.1051/0004-6361/201118367

Scepi, N., Begelman, M. C., and Dexter, J. (2021). Magnetic flux inversion in a peculiar changing look AGN. *MNRAS* 502, L50–L54. doi:10.1093/mnrasl/slab002

Schnittman, J. D., and Krolik, J. H. (2010). X-Ray polarization from accreting black holes: coronal emission. *ApJ* 712, 908–924. doi:10.1088/0004-637X/712/2/908

Shankar, F., Salucci, P., Granato, G. L., De Zotti, G., and Danese, L. (2004). Supermassive black hole demography: the match between the local and accreted mass functions. *MNRAS* 354, 1020–1030. doi:10.1111/j.1365-2966.2004.08261.x

Shankar, F., Weinberg, D. H., Marsden, C., Grylls, P. J., Bernardi, M., Yang, G., et al. (2020). Probing black hole accretion tracks, scaling relations, and radiative efficiencies from stacked X-ray active galactic nuclei. *MNRAS* 493, 1500–1511. doi:10.1093/mnras/stz3522

Shankar, F., Weinberg, D. H., and Miralda-Escudé, J. (2009). Self-consistent models of the AGN and black hole populations: duty cycles, accretion rates, and the mean radiative efficiency. *ApJ* 690, 20–41. doi:10.1088/0004-637X/690/1/20

Shappee, B. J., Prieto, J. L., Grupe, D., Kochanek, C. S., Stanek, K. Z., De Rosa, G., et al. (2014). The man behind the curtain: X-rays drive the UV through NIR variability in the 2013 active galactic nucleus outburst in NGC 2617. *ApJ* 788, 48. doi:10.1088/0004-637X/788/1/48

Sironi, L., and Beloborodov, A. M. (2020). Kinetic simulations of radiative magnetic reconnection in the coronae of accreting black holes. *ApJ* 899, 52. doi:10.3847/1538-4357/aba622

Smith, K. L., Mushotzky, R. F., Vogel, S., Shimizu, T. T., and Miller, N. (2016). Radio properties of the BAT AGNs: the FIR-radio relation, the fundamental plane, and the main sequence of star formation. *ApJ* 832, 163. doi:10.3847/0004-637X/832/2/163

Sniegowska, M., Czerny, B., Bon, E., and Bon, N. (2020). Possible mechanism for multiple changing-look phenomena in active galactic nuclei. *A&A* 641, A167. doi:10.1051/0004-6361/202038575

Soltan, A. (1982). Masses of quasars. *MNRAS* 200, 115–122. doi:10.1093/mnras/200.1.115

Sridhar, N., Sironi, L., and Beloborodov, A. M. (2021). Comptonization by reconnection plasmoids in black hole coronae I: magnetically dominated pair plasma. *MNRAS* 507, 5625–5640. doi:10.1093/mnras/stab2534

Sridhar, N., Sironi, L., and Beloborodov, A. M. (2023). Comptonization by reconnection plasmoids in black hole coronae II: electron-ion plasma. *MNRAS* 518, 1301–1315. doi:10.1093/mnras/stac2730

Stern, B. E., Poutanen, J., Svensson, R., Sikora, M., and Begelman, M. C. (1995). On the geometry of the X-ray–emitting region in Seyfert galaxies. *ApJ* 449, L13. doi:10.1086/309617

Stern, D., McKernan, B., Graham, M. J., Ford, K. E. S., Ross, N. P., Meisner, A. M., et al. (2018). A mid-IR selected changing-look quasar and physical scenarios for abrupt AGN fading. *ApJ* 864, 27. doi:10.3847/1538-4357/aac726

Svensson, R. (1984). Steady mildly relativistic thermal plasmas - processes and properties. *MNRAS* 209, 175–208. doi:10.1093/mnras/209.2.175

Tagliacozzo, D., Marinucci, A., Ursini, F., Matt, G., Bianchi, S., Baldini, L., et al. (2023). The geometry of the hot corona in MCG-05-23-16 constrained by X-ray polarimetry. arXiv e-prints, Available at: https://doi.org/10.48550/arXiv.2305.10213.

Tamborra, F., Matt, G., Bianchi, S., and Dovčiak, M. (2018). MoCA: a Monte Carlo code for Comptonisation in Astrophysics. I. Description of the code and first results. *A&A* 619, A105. doi:10.1051/0004-6361/201732023

Tashiro, M., Maejima, H., Toda, K., Kelley, R., Reichenthal, L., Lobell, J., et al. (2018). "Concept of the X-ray astronomy recovery mission," in *Space telescopes and instrumentation 2018: ultraviolet to gamma ray*. Editors J.-W. A den Herder, S Nikzad, and K Nakazawa. vol. 10699 of Society of Photo-Optical Instrumentation Engineers (SPIE) Conference Series. doi:10.1117/12.2309455

Tazaki, F., Ueda, Y., Terashima, Y., and Mushotzky, R. F. (2011). Suzaku view of the Swift/BAT active galactic nuclei. IV. Nature of two narrow-line radio galaxies (3C 403 and IC 5063). *ApJ* 738, 70. doi:10.1088/0004-637X/738/1/70

Tetarenko, B. E., Sivakoff, G. R., Heinke, C. O., and Gladstone, J. C. (2016). WATCHDOG: a comprehensive all-sky Database of galactic black hole X-ray binaries. *ApJS* 222, 15. doi:10.3847/0067-0049/222/2/15

Titarchuk, L. (1994). Generalized comptonization models and application to the recent high-energy observations. *ApJ* 434, 570. doi:10.1086/174760

Titarchuk, L., and Lyubarskij, Y. (1995). Power-law spectra as a result of comptonization of the soft radiation in a plasma cloud. *ApJ* 450, 876. doi:10.1086/176191

Tomsick, J., Zoglauer, A., Sleator, C., Lazar, H., Beechert, J., Boggs, S., et al. (2019). The Compton spectrometer and imager. *Bull. Am. Astronomical Soc.* 51, 98. doi:10.48550/arXiv.1908.04334

Tonry, J. L., Denneau, L., Heinze, A. N., Stalder, B., Smith, K. W., Smartt, S. J., et al. (2018). ATLAS: a high-cadence all-sky survey system. *PASP* 130, 064505. doi:10.1088/1538-3873/aabadf

Tortosa, A., Bianchi, S., Marinucci, A., Matt, G., and Petrucci, P. O. (2018). A NuSTAR census of coronal parameters in Seyfert galaxies. *A&A* 614, A37. doi:10.1051/0004-6361/201732382

Tortosa, A., Ricci, C., Ho, L. C., Tombesi, F., Du, P., Inayoshi, K., et al. (2023). Systematic broad-band X-ray study of super-Eddington accretion on to supermassive

black holes - I. X-ray continuum. *MNRAS* 519, 6267–6283. doi:10.1093/mnras/stac3590

Trakhtenbrot, B., Arcavi, I., MacLeod, C. L., Ricci, C., Kara, E., Graham, M. L., et al. (2019). 1ES 1927+654: an AGN caught changing look on a timescale of months. *ApJ* 883, 94. doi:10.3847/1538-4357/ab39e4

Urry, C. M., and Padovani, P. (1995). Unified schemes for radio-loud active galactic nuclei. *PASP* 107, 803. doi:10.1086/133630

Ursini, F., Bassani, L., Malizia, A., Bazzano, A., Bird, A. J., Stephen, J. B., et al. (2019). The coronal temperature of NGC 4388 and NGC 2110 measured with INTEGRAL. *A&A* 629, A54. doi:10.1051/0004-6361/201936273

Ursini, F., Marinucci, A., Matt, G., Bianchi, S., Marin, F., Marshall, H. L., et al. (2023). Mapping the circumnuclear regions of the Circinus galaxy with the imaging X-ray polarimetry explorer. *MNRAS* 519, 50–58. doi:10.1093/mnras/stac3189

Ursini, F., Petrucci, P. O., Matt, G., Bianchi, S., Cappi, M., De Marco, B., et al. (2016). High-energy monitoring of NGC 4593 with XMM-Newton and NuSTAR. X-ray spectral analysis. *MNRAS* 463, 382–392. doi:10.1093/mnras/stw2022

Uttley, P., Cackett, E. M., Fabian, A. C., Kara, E., and Wilkins, D. R. (2014). X-ray reverberation around accreting black holes. *A&ARv* 22, 72. doi:10.1007/s00159-014-0072-0

Vaiana, G. S., and Rosner, R. (1978). Recent advances in coronal physics. *ARA&A* 16, 393–428. doi:10.1146/annurev.aa.16.090178.002141

Vasudevan, R. V., and Fabian, A. C. (2007). Piecing together the X-ray background: bolometric corrections for active galactic nuclei. *MNRAS* 381, 1235–1251. doi:10.1111/j.1365-2966.2007.12328.x

Walton, D. J., Baloković, M., Fabian, A. C., Gallo, L. C., Koss, M., Nardini, E., et al. (2021). Extreme relativistic reflection in the active galaxy ESO 033-G002. *MNRAS* 506, 1557–1572. doi:10.1093/mnras/stab1290

Walton, D. J., Reis, R. C., Cackett, E. M., Fabian, A. C., and Miller, J. M. (2012). The similarity of broad iron lines in X-ray binaries and active galactic nuclei. *MNRAS* 422, 2510–2531. doi:10.1111/j.1365-2966.2012.20809.x

Walton, D. J., Risaliti, G., Harrison, F. A., Fabian, A. C., Miller, J. M., Arevalo, P., et al. (2014). NuSTAR and XMM-Newton observations of NGC 1365: extreme absorption variability and a constant inner accretion disk. *ApJ* 788, 76. doi:10.1088/0004-637X/788/1/76

Wambsganss, J. (2006). "Part 4: gravitational microlensing," in *Saas-fee advanced course 33: gravitational lensing: strong, weak and micro*. Editors G Meylan, P Jetzer, P North, P Schneider, C. S Kochanek, and J Wambsganss, 453–540.

Weisskopf, M. C., Soffitta, P., Baldini, L., Ramsey, B. D., O'Dell, S. L., Romani, R. W., et al. (2022). Imaging X-ray polarimetry explorer: prelaunch. *J. Astronomical Telesc. Instrum. Syst.* 8, 026002. doi:10.1117/1.JATIS.8.2.026002

Wen, S., Jonker, P. G., Stone, N. C., Zabludoff, A. I., and Psaltis, D. (2020). Continuum-fitting the X-ray spectra of tidal disruption events. *ApJ* 897, 80. doi:10.3847/1538-4357/ab9817

Wevers, T. (2020). Fainter harder brighter softer: a correlation between α_{ox}, X-ray spectral state, and Eddington ratio in tidal disruption events. *MNRAS* 497, L1–L6. doi:10.1093/mnrasl/slaa097

Wevers, T., Pasham, D. R., van Velzen, S., Miller-Jones, J. C. A., Uttley, P., Gendreau, K. C., et al. (2021). Rapid accretion state transitions following the tidal disruption event AT2018fyk. *ApJ* 912, 151. doi:10.3847/1538-4357/abf5e2

Wilkins, D. R., Cackett, E. M., Fabian, A. C., and Reynolds, C. S. (2016). Towards modelling X-ray reverberation in AGN: piecing together the extended corona. *MNRAS* 458, 200–225. doi:10.1093/mnras/stw276

Wilkins, D. R., and Fabian, A. C. (2011). Determination of the X-ray reflection emissivity profile of 1H 0707-495. *MNRAS* 414, 1269–1277. doi:10.1111/j.1365-2966.2011.18458.x

Wilkins, D. R., and Fabian, A. C. (2012). Understanding X-ray reflection emissivity profiles in AGN: locating the X-ray source. *MNRAS* 424, 1284–1296. doi:10.1111/j.1365-2966.2012.21308.x

Wilkins, D. R., and Fabian, A. C. (2013). The origin of the lag spectra observed in AGN: reverberation and the propagation of X-ray source fluctuations. *MNRAS* 430, 247–258. doi:10.1093/mnras/sts591

Wilkins, D. R., and Gallo, L. C. (2015). Driving extreme variability: the evolving corona and evidence for jet launching in Markarian 335. *MNRAS* 449, 129–146. doi:10.1093/mnras/stv162

Wilms, J., Allen, A., and McCray, R. (2000). On the absorption of X-rays in the interstellar medium. *ApJ* 542, 914–924. doi:10.1086/317016

XRISM Science Team (2022). *XRISM quick reference*. arXiv e-prints, Available at: https://doi.org/10.48550/arXiv.2202.05399.

Yao, Y., Lu, W., Guolo, M., Pasham, D. R., Gezari, S., Gilfanov, M., et al. (2022). The tidal disruption event AT2021ehb: evidence of relativistic disk reflection, and rapid evolution of the disk-corona system. *ApJ* 937, 8. doi:10.3847/1538-4357/ac898a

Yu, Q., and Tremaine, S. (2002). Observational constraints on growth of massive black holes. *MNRAS* 335, 965–976. doi:10.1046/j.1365-8711.2002.05532.x

Zdziarski, A. A., Johnson, W. N., and Magdziarz, P. (1996). Broad-band γ-ray and X-ray spectra of NGC 4151 and their implications for physical processes and geometry. *MNRAS* 283, 193–206. doi:10.1093/mnras/283.1.193

Zdziarski, A. A., Jourdain, E., Lubiński, P., Szanecki, M., Niedźwiecki, A., Veledina, A., et al. (2021). Hybrid comptonization and electron-positron pair production in the black-hole X-ray binary MAXI J1820+070. *ApJ* 914, L5. doi:10.3847/2041-8213/ac0147

Zdziarski, A. A., and Lightman, A. P. (1985). Nonthermal electron-positron pair production and the 'universal' X-ray spectrum of active galactic nuclei. *ApJ* 294, L79–L83. doi:10.1086/184513

Zdziarski, A. A., Lightman, A. P., and Maciolek-Niedzwiecki, A. (1993). Acceleration efficiency in nonthermal sources and the soft gamma rays from NGC 4151 observed by OSSE and SIGMA. *ApJ* 414, L93. doi:10.1086/187004

Zhang, S., Santangelo, A., Feroci, M., Xu, Y., Lu, F., Chen, Y., et al. (2019a). The enhanced X-ray Timing and Polarimetry mission—eXTP. *Sci. China Phys. Mech. Astronomy* 62, 29502. doi:10.1007/s11433-018-9309-2

Zhang, W., Dovčiak, M., and Bursa, M. (2019b). Constraining the size of the corona with fully relativistic calculations of spectra of extended coronae. I. The Monte Carlo radiative transfer code. *ApJ* 875, 148. doi:10.3847/1538-4357/ab1261

Zhang, X., and Lu, Y. (2017). On the mean radiative efficiency of accreting massive black holes in AGNs and QSOs. *Sci. China Phys. Mech. Astronomy* 60, 109511. doi:10.1007/s11433-017-9062-1

Zoghbi, A., Matt, G., Miller, J. M., Lohfink, A. M., Walton, D. J., Ballantyne, D. R., et al. (2017). A long look at MCG-5-23-16 with NuSTAR. I. Relativistic reflection and coronal properties. *ApJ* 836, 2. doi:10.3847/1538-4357/aa582c